PNAS

Supporting Information for

Restoring neuronal iron homeostasis revitalizes neurogenesis after spinal cord injury

Huimin Geng[a,b,1], Zhiwei Li[b,c,1], Zheng Li[b,c], Yuqi Zhang[b], Zhiliang Gao[a], Lei Sun[d], Xingang Li[b], Shilei Ni[b,c,2], Jiwei Cui[a,2], and Jingcheng Hao[a,2]

[a]Key Laboratory of Colloid and Interface Chemistry of the Ministry of Education, School of Chemistry and Chemical Engineering, Shandong University, Jinan, Shandong 250100, China
[b]Department of Neurosurgery, Qilu Hospital of Shandong University, Institute of Brain and Brain-Inspired Science, Cheeloo College of Medicine, Shandong University, Jinan, Shandong 250012, China
[c]Shandong Key Laboratory of Brain Function Remodeling, Jinan, Shandong 250117, China
[d]Department of Endocrinology, Qilu Hospital of Shandong University, Cheeloo College of Medicine, Shandong University, Jinan, Shandong 250012, China.

Author contributions: H.G., X.L., S.N., J.C., and J.H. designed research; H.G., Zhiwei Li, Zheng Li, Y.Z., and Z.G. performed research; S.N. and J.C. contributed new reagents/analytic tools; H.G., Zhiwei Li, Zheng Li, L.S., X.L., S.N., J.C., and J.H. analyzed data; and H.G., Zhiwei Li, S.N., J.C., and J.H. wrote the paper.

Competing Interest Statement:
The authors declare no competing interests.
[1]H.G. and Zhiwei Li contributed equally to this work.
[2]To whom correspondence may be addressed. Email: nishilei@sdu.edu. cn (S. Ni), jwcui@sdu.edu.cn (J. Cui) and jhao@sdu.edu.cn (J. Hao)

Table of contents:

Section 1: Supplementary Materials and Methods 3
1. Preparation and characterization of PDAR NPs 3
2. Rheological measurements 3
3. Analysis of iron ion adsorption *in vitro* 3
4. Antioxidant measurements 3
5. *In vitro* PDAR release 4
6. Adhesive strength test of hydrogels 4
7. Compression test of hydrogels 4
8. *In vivo* degradation test 4
9. Cell culture of PC12 cells 4
10. Cell culture of DRG neurons 4
11. Cell culture of NSPCs 5
12. Live/dead cell staining and cell viability assay 5
13. Intracellular uptake of hydrogel complexes 5
14. Intracellular iron detection 6
15. Lipid peroxidation assessment 6
16. Measurement of ROS level 6
17. Measurement of GSH level 7
18. Injection of ferrous iron into spinal cords 7
19. Western blotting 7
20. Quantitative RT-PCR 8
21. MRI evaluation 8
22. Locomotor function assessments 8
23. Electrophysiological analysis 8
24. RNA sequencing and bioinformatics analysis 9
25. BrdU administration 9
26. Immunofluorescence staining 9
27. Characterization of inflammatory cytokines 9
28. Identification of microglia/macrophage phenotype 10
29. Statistical analysis 10
Section 2. Figs. S1–S36 and Table S1 11
Section 3. Legends for Movies S1–S3 51
Section 4. SI References 52

Section 1: Supplementary Materials and Methods

1. Preparation and characterization of PDAR NPs

Briefly, 100 mg of dopamine hydrochloride (98%, Sigma-Aldrich, USA) was dissolved in 110 mL of Milli-Q water, followed by stirring for 10 min. 100 mg of arginine (J&K Chemical Ltd., China) was dissolved in 10 mL of water and added dropwise to the dopamine solution, followed by stirring for 12 h at 25 °C. The color of the solution turned into brown gradually and subsequently dark brown. The products were obtained by centrifugation (10000 *g* for 10 min) and washed with water three times. The diameter and zeta potential of PDAR NPs were obtained by a Zetasizer instrument (Malvern, Nano ZS90, England). The morphology of PDAR NPs were characterized using transmission electron microscopy (TEM, JEM-1400, Japan) images.

2. Rheological measurements

A rheometer (HAAKE RS6000, Germany) with a cone–plate system (C35/1° Ti L07116, diameter 35 mm, and core angle 1°) was used to evaluate the rheological behavior of the hydrogels. The *G′* and *G″* of the hydrogels were detected as a function of frequency sweeps (0.1–100 Hz) at a strain level of 1%. The viscoelasticity was detected using an oscillatory frequency sweep of 0.1 Hz–1000 Hz. To quantitatively examine the self-healing property of TPC hydrogels, the stress amplitude sweep method was used. Amplitude oscillatory force was switched from 1 Pa (100 s for each interval) to 1000 Pa (60 s for each interval).

3. Analysis of iron ion adsorption *in vitro*

The capacity of iron ion adsorption was examined by by Resonance Raman spectroscopy using a LabRAM HR800 Evolution (Horiba, Japan) equipped with a 633 nm laser (NIR diode). CC solution, TC and TPC hydrogels (0.5 mL) were mixed with 2 mL of $FeCl_3$ solution (100 mM), followed by incubation for 24 h. Hydrogels were washed with water three times and freeze-dried before analysis. The Fe contents in hydrogels were determined by ICP-MS (Shimadzu, 2030, Japan).

4. Antioxidant measurements

The *in vitro* antioxidant efficacy of the PDAR NPs was evaluated by scavenging the 2,2-diphenyl-1-(2,4,6-trinitrophenyl) hydrazyl (DPPH, Sigma-Aldrich, USA) free radicals. A 10 mg of DPPH was dissolved in 100 mL of ethanol. Afterward, the desired amount of PDAR samples (5, 10, 20, 30, 40, and 50 μg) were dispersed in 3 mL of ethanol. A 0.5 mL of PDAR suspension was mixed with 3.5 mL of DPPH solution. A 0.5 mL of water mixed with 3.5 mL of DPPH solution was used as a positive control group. A 0.5 mL of PDAR solution mixed with 3.5 mL of ethanol was used as a negative control group. The mixture was incubated under stirring in dark for 30 min. The absorption at 517 nm was scanned by using a UV–vis spectrophotometer (Shimadzu UV2600, Japan). The degradation of DPPH was calculated by the following equation:

$$\text{DPPH scavenging \%} = [1- (A_{sample}-A_{negative})/A_{positive}] \times 100\% \quad (1)$$

where A_{sample}, $A_{negative}$, and $A_{positive}$ are the absorption intensity of the sample, positive control, and negative control groups, respectively.

The DPPH scavenging ability of CC, TC, and TPC was measured similarly. Specifically, the

samples were homogenized before examination.

5. *In vitro* PDAR release

PDAR NPs were fluorescently labelled by incubation of PDAR NPs with FITC for 4 h at 25 °C, followed by washing with water three times. The TPC hydrogels (500 μL) loaded with FITC-labelled PDAR NPs (100 μg mL^{-1}) were prepared in a 5 mL centrifuge tube. After complete gelation, 3 mL of PBS (10 mM, pH 7.4) was added into each tube at 37 °C. After a predetermined time, 0.1 mL of the release buffer was removed for analysis. Subsequently, 1 mL of fresh buffer was added into the tube to maintain a constant volume. The concentration of the PDAR NPs released from hydrogels was analyzed by a fluorescence spectrophotometer (HITACHI F-7100, Japan).

6. Adhesive strength test of hydrogels

The adhesion of hydrogels to the host tissue was tested by using fresh porcine skin. Briefly, the porcine skin was cut into a 15 mm × 25 mm rectangle and kept clean before use. TPC hydrogels were applied onto the surface of porcine skin and another skin was put onto the hydrogel. The adhesive area was 15 mm × 15 mm. The adhesion strength was tested using the lap shear test on a universal material testing machine (Instron 3344, USA) equipped with a 50 N load cell at a rate of 2 mm min^{-1}.

7. Compression test of hydrogels

The cylindrical TPC hydrogels (10*10*10 mm^3) were used for compression tests by using a universal material testing machine (Instron 3344, USA) equipped with a 50 N load cell at a rate of 5 mm min^{-1}.

8. *In vivo* degradation test

To visually monitor the degradation process of hydrogels *in vivo*, FITC-labeled CC was used to prepare CC solution, TC and TPC hydrogels. The hydrogels (100 μL) were injected subcutaneously into 6-week-old nude mice (SPF Biotechnology, China). At predetermined time points, all animals were imaged with an *in vivo* imaging system (IVIS) Spectrum Instrument (PerkinElmer, USA). The fluorescence semi-quantitative analysis was carried out with the Living Imaging software.

9. Cell culture of PC12 cells

PC12 cells were derived from transplantable male rat adrenal pheochromocytoma. The cells with expression of nerve growth factor (NGF) receptors were typically used as an alternative for primary neurons. In this study, PC12 cells with passed related genetic identification and microbiological detection were provided by Cell Bank/Stem Cell Bank, Chinese Academy of Sciences. PC12 cells were incubated in RPMI 1640 medium (Gibco, USA) supplemented with 10% fetal bovine serum (FBS, Gibco, USA) for proliferation or supplemented with 2% FBS and 100 ng mL^{-1} NGF (Sigma-Aldrich, USA) for differentiation.

10. Cell culture of DRG neurons

DRG neurons were isolated from day 3 postnatal Sprague-Dawley (SD) rats and incubated in

collagenase I (1.25 mg mL^{-1}, Macklin, China) for 60 min followed by trypsinization (0.25%, Solarbio, China) for 15 min at 37 °C. The dispersed DRG neurons were plated onto poly-L-lysine (M_w 150-300 kDa, 10 μg mL^{-1}, Sigma-Aldrich, USA) coated glass coverslips and cultured in DMEM/F12 (1:1, Gibco, USA) supplemented with 10% FBS and 100 ng mL^{-1} NGF. After 24 h incubation, cells were treated with Neurobasal medium (Gibco, USA) supplemented with 2% B27 (Gibco, USA), 2% GlutaMAX (Gibco, USA), and 100 ng mL^{-1} NGF for the culture of neuron cells. All the cells were cultured at 37 °C with 5% CO_2 in a humidified cell incubator. As shown in the inset image of Fig. 1H, Sholl intersection profile is obtained by counting the number of dendritic branches at a given distance from the soma using an imaginary sphere with a given radius. To intuitive comparison of complex dendritic structures, the branching complexity of neurons was given by the shaded areas of Sholl intersections, as reported previously (1,2).

11. Cell culture of NSPCs

NSPCs were excised from the cerebral cortex of E14 embryos (SD rats). Briefly, after the meninges were removed, the tissue was digested by ACCUTASE (Gibco, USA) for 20 min at 37 °C, followed by centrifugation at 300 *g*. The tissue was resuspended in serum-free DMEM/F12 (1:1) supplemented with 2% B27, 2% GlutaMAX, 20 ng mL^{-1} basic fibroblast growth factor (bFGF, Peprotech, USA), and 20 ng mL^{-1} epidermal growth factor (EGF, Peprotech, USA) and filtered using a 40 μm cell filter strainer. The neurospheres were passaged every 7 days and 30% of total medium was refreshed every 2 days.

For differentiation, the neurospheres were dissociated into single cells with ACCUTASE. These cells were plated onto 10 μg mL^{-1} poly-L-lysine-coated 6-well plates and cultured in DMEM/F12 (1:1, Gibco, USA) supplemented with 1% FBS, 2% B27, and 2% GlutaMAX. 10 μM $FeSO_4 \cdot 7H_2O$ and 20 μL of hydrogels were added to 1 mL of differentiation medium. After culture for 7 days, the differentiated NSPCs were used for further experiments.

12. Live/dead cell staining and cell viability assay

Live/dead cell staining was performed following the protocols described by the manufacturer (Beyotime, China). Briefly, calcein AM (1:1000, Ex/Em=494/517 nm) and propidium iodide (PI, 1:1000, Ex/Em=535/617 nm) were added to the culture medium, followed by incubation for 30 min at 37°C. Cells were washed three times with PBS and visualized using CLSM (Leica TCS SP8, Germany). For quantitative analysis of the cell viability, Cell Counting Kit-8 (CCK-8, Dojindo, Japan) was used according to the manufacturer's instructions. Briefly, 10 μL of CCK-8 solution was added to the 90 μL of culture medium in each well of 96-well plates, followed by incubation for 1 h at 37 °C. The absorbance of each well at 450 nm was measured using a multimode plate reader (Ensight™, PerkinElmer, USA).

13. Intracellular uptake of hydrogel complexes

To evaluate intracellular uptake of hydrogel complexes, FITC-CC was used to prepare the fluorescent CC scaffold, TC hydrogels, and TPC hydrogels. Hydrogel extracts were prepared by immersing 20 μL of hydrogels in 1 mL of cell culture medium for 24 h at 37 °C. PC12 cells were incubated in the solution of hydrogel extracts for another 24 h at 37°C. After the incubation, cells were washed with PBS three times and visualized using CLSM (Leica TCS SP8, Germany).

14. Intracellular iron detection

To detect intracellular Fe^{2+} levels, FerroOrange (Dojindo, Japan) was used according to the manufacturer's instructions. After the incubation with RSL3 (0.5 μM) and hydrogel extracts (20 μL) for 24 h, PC12 cells were stained with 1 μM FerroOrange (Ex/Em = 543/580 nm), 2.5 μg mL^{-1} WGA-AF633 (Invitrogen, USA) (Ex/Em = 632/647 nm), and Hoechst 33342 (1:100, Beyotime, China) (Ex/Em = 350/461 nm). Images were acquired using CLSM (Leica TCS SP8, Germany).

An iron colorimetric assay kit (Applygen, China) was used to evaluate the total iron level of cells and tissues according to the manufacturer's protocol. Briefly, samples were incubated with 200 μL of cell lysis buffer for 2 h in 24-well plates. The lysed samples were furhter incubated with isometric assay buffer containing 2.25% $KMnO_4$ for 1 h at 60 °C. After cooling to 25 °C, the samples were incubated with 30 μL of the iron probe for 30 min. The absorbance (550 nm) of supernatants was measured using the multimode plate reader (Ensight™, PerkinElmer, USA). The iron level was normalized by protein levels of samples through a BCA protein assay kit (Beyotime, China).

DAB-enhanced Prussian blue iron staining was performed to detect the iron level of injured spinal cords. At 7 dpi, the cross-sections of the injured epicenter were treated with Prussian blue staining solution containing 1% potassium ferrohydride and 1% hydrochloric acid for 30 min, followed by DAB staining, nucleus staining, dehydration, and sealing.

15. Lipid peroxidation assessment

Lipid peroxidation levels of cells and injured spina cords at 3 dpi were evaluated using an malonaldehyde (MDA) assay kit (Beyotime, China) following the manufacturer's instructions. Briefly, PC12 cells were incubated with 0.5 μM RSL3 and CC, TC, TPC hydrogel extracts, respectively, for 12 h. The lysis buffer was added to the cells or the spinal cords (0.5 cm length) on ice and the homogenized mixture was centrifuged at 12000 *g* for 10 min at 4 °C to obtain the supernatant. 100 μL of each supernatant was futher incubated with 100 μL of MDA testing solution containing thiobarbituric acid (TBA) and antioxidant for 15 min at 100 °C. After cooling to 25 °C, the samples were centrifuged at 1000 *g* for 10 min and the supernatant was collected to measure the absorbance (532 nm) using a multimode plate reader (Ensight™, PerkinElmer, USA). The MDA content was normalized by protein levels of tissues through a BCA protein assay kit.

16. Measurement of ROS level

The intracellular ROS level was measured using 2', 7'-dichlorofluorescein-diacetate (DCFH-DA, Beyotime, China). Briefly, PC12 cells were incubated with 0.5 μM RSL3 and hydrogel extracts for 12 h, followed by incubation with 10 μM DCFH-DA for 20 min at 37 °C. Fluorescence images (Ex/Em=488/525 nm) were obtained by using CLSM (Leica TCS SP8, Germany). For quantitative analysis by using flow cytometry (BD Accuri™ C6 cytometry, USA), cells were digested by 0.25% trypsin, centrifuged at 300 *g* for 5 min, resuspended by flow cytometry staining buffer before analysis.

The tissue ROS level was detected using BBoxiProbe® O11 (BestBio, China) which could be

oxidized to green fluorescent materials by ROS. According to the manufacturer's protocol, 5 mm of the fresh spinal cord was removed from the injured epicenter. After washing three times with PBS, the tissues were homogenized in the lysis buffer followed by centrifugation at 100 *g* for 5 min to collect the supernatant. Then, 190 μL of homogenized supernatant was incubated with 10 μL of O11 probes in dark for 20 min at 37 °C. Multimode plate reader (Ensight™, PerkinElmer, USA) was used to detect the fluorescent intensity of samples (Ex/Em=488/530 nm) and the data were normalized by protein levels of tissues.

H_2O_2 level was measured using a H_2O_2 assay kit (Beyotime, China) following the manufacturer's instructions. Briefly, 200 μL of lysis buffer was added to samples on ice. Subsequently, the homogenized solution was centrifuged at 12000 *g* for 5 min at 4 °C to obtain the supernatants. In a 96-well plate, 50 μL of supernatants were incubated with 100 μL of H_2O_2 detecting assays at 25 °C for 30 min. The absorbance at 560 nm was measured using a multimode plate reader (Ensight™, PerkinElmer, USA). The data were normalized by protein levels of samples.

17. Measurement of GSH level

The GSH assay kit (Beyotime, China) was used to detect the GSH level of cells and injured spinal cords. Briefly, samples were treated with protein removal reagent M solution with a volume ratio of 1:3 (samples to M solution) and lysed by fast freezing-thawing processes. After centrifugation at 10000 *g* for 10 min at 4 °C, 10 μL supernatants were then transferred to a 96-well plate and mixed with 150 μL GSH detecting working solution containing 5,5'-dithiobis-(2-nitrobenzoic acid) (DTNB) at RT for 5 min. The absorbance at 412 nm was measured using a multimode plate reader (Ensight™, PerkinElmer, USA) and the data were normalized by protein levels of samples.

18. Injection of ferrous iron into spinal cords

Animals were anesthetized with isoflurane. Following laminectomy, the dorsal surface of the T10 spinal cord was exposed. With or without SCI treatments, 5 μL of ferrous ions were injected into the center of injured or uninjured spinal cords at an angle of 90° using a microsyringe with an injection depth of 1.0 mm and speed of 0.3 uL min^{-1}. Blood vessels were avoided during injection. After injection, the needle was left in place for 5 min to prevent leakage and then slowly withdrawn. Subsequently, TPC hydrogels were applied onto the dorsal surface of the injured spinal cord, followed by incision close. In this study, fresh $FeSO_4 \cdot 7H_2O$ (800 mM) was used in the eFe group, and fresh $FeSO_4 \cdot 7H_2O$ (80 mM) was used in the mFe group. Moreover, 5 μL of saline was injected as a control group.

19. Western blotting

Spinal cords (5 mm length) at 3 dpi were removed from the injured epicenter. The samples were lysed in RIPA buffer (Beyotime, China) supplemented with protease inhibitor PMSF (Solarbio, China) for 30 min at 4 °C. After sonication, centrifugation, and heating of the lysed samples, equal quantities (20 μg) of protein extracts were subjected to 10% SDS-PAGE and transferred to polyvinylidene fluoride (PVDF) membranes for western blotting. The following antibodies were used for staining: IRP2 (1:1000, ab181153, Abcam, UK), TfR1 (1:1000, ab269513, Abcam, UK), Ferritin (1:1000, ab75973, Abcam, UK), TF (1:1000, ab82411, Abcam,

UK), xCT (1:1000, ab175186, Abcam, UK), GPX4 (1:1000, ab125066, Abcam, UK), and GAPDH (1:10000, #5174, CST, USA).

20. Quantitative RT-PCR

Total RNA was extracted from cells and tissues using TRIzol reagent (Thermo Fisher Scientific, USA). 1 μg of total RNA was reverse-transcribed into complementary DNA (cDNA) using a ReverTra Ace qPCR RT Kit (TOYOBO, Japan). RT-qPCR was performed with TB Green Premix Ex Taq (Takara, Japan) on a 480II Real-Time PCR Detection System (Roche, Switzerland). Three independent replicates were conducted for each specimen. GAPDH was used to normalize the mRNA expression. All the primer sequences were presented in Table S1.

21. MRI evaluation

MRI experiments were conducted on a 3.0 Tesla MR scanner (Siemens, MAGNETOM Verio 3.0, Germany) with a wrist coil. After anesthetization of rats at 3 dpi, fat-suppressed sagittal and axial T2-weighted turbo spin-echo images (T2WI) of thoracic vertebra were acquired with the following parameters: repetition time (TR) = 2200 ms; echo time (TE) = 63 ms; slice thickness = 1.5 mm; field of view (FOV) = 120 mm × 120 mm; average = 2.

22. Locomotor function assessments

BBB test was performed in the open field at 0, 1, 3, 7, 14, 21, 28, 35, 42, 49, and 56 dpi to semi-quantitatively analyze the voluntary movements of hindlimbs. The scores were evaluated separately by two unwitting examiners, ranging from 0 (complete paralysis) to 21 (normal locomotion).

As a supplementary study of BBB score, an inclined plane test was used to evaluate the animal grip at 4 and 8 wpi. The rats were placed on the inclined plate with a rubber pad, and the longitudinal axis of a rat was kept parallel to the longitudinal axis of the inclined plate. Subsequently, the height of the inclined plate was slowly raised to the maximum angle, where the rat could stay on the inclined plate for 5 s. Each rat was measured three times and the average value was used.

For the footprint analysis, the forepaws and hindpaws of animals were stained with red and blue ink on the test day at 8 wpi, respectively. They were placed onto the runway (60 × 10 cm) covered with white paper to track the footprints. The rotation angle was measured as the angle of the hindpaw axis relative to the runway axis. The base of support was defined as the spacing between the left and right hindpaws. The stride length was determined as the distance of hindpaw movement in a step cycle. The relative position was represented between the forepaws and hindpaws. The footprints of hindpaws tend to overlap those of forepaws during walking for healthy animals.

23. Electrophysiological analysis

Electrophysiology examinations were performed to evaluate the functional status of sensorimotor signal conduction at 8 wpi. Briefly, the sensorimotor cortex (SMC) and sciatic nerve of animals were exposed after anesthesia. To record the MEP, the stimulating electrode was inserted into the SMC while the recording electrode was inserted into the sciatic nerve.

The stimulus voltage and pulse width were 42 V and 0.2 ms, respectively. On the contrary, the stimulating electrode was inserted into the sciatic nerve while the recording one was inserted into the SMC to record SEP using 32 mA of stimulus current. The waveforms, amplitude, and latency of MEP and SEP were acquired and analyzed.

24. RNA sequencing and bioinformatics analysis

TRIzol reagent was used to extract total RNA from the injured spinal cord (5 mm) in the SCI and TPC groups at 7 dpi (n = 4). Total RNA was isolated using the RNeasy mini kit (Qiagen, Germany) and RNA-Seq libraries were prepared using the NEBNext UltraTM RNA Library Prep Kit for Illumina (NEB, USA) through paired-end (240 base paired-end reads) sequencing on the Agilent Bioanalyzer 2100 system (Agilent Technologies, CA, USA). Raw data were quality filtered to generate “clean reads” for further analysis. The differentially expressed genes (P-value ≤ 0.05, |Fold Change| ≥ 1.2) were subjected to the enrichment analysis of GO and KEGG by using the OmicShare tools (https://www.omicshare.com/tools).

25. BrdU administration

Newborn cells were labelled *in vivo* through intraperitoneal injection of BrdU (Sigma, USA) at a daily dose of 100 mg kg^{-1} for the indicated duration.

26. Immunofluorescence staining

Samples were fixed with 4% paraformaldehyde for 15 min and incubated in 0.3% Triton X-100 for 15 min at 25°C. After blocking with 10% normal goat serum (ZSGB-bio, China) for 1 h, the slices were incubated with primary antibodies for X h at 4 °C. Subsequently, the samples were subjected to AF488- or AF594-conjugated secondary antibodies (ZSGB-bio, China) for 1 h and DAPI (Beyotime, China) for 15 min. Antifade mounting medium (Beyotime, China) was added to the sections for imaging using CLSM (Leica TCS SP8, Germany) and panoramic digital section scanning microscopy (Olympus VS120, Japan). Fluorescence semi-quantitative analysis was conducted by ImageJ software (version 1.53c). The following primary antibodies were used for staining: rabbit anti-DCX (1:1000, ab18723, Abcam, UK), mouse anti-Tuj-1 (1:1000, ab78078, Abcam, UK), mouse anti-Ki67 (1:200, ab279653, Abcam, UK), rabbit anti-SOX2 (1:200, ab92494, Abcam, UK), rabbit anti-GAP43 (1:200, #8945, CST, USA), rabbit anti-Iba1 (1:200, ab178847, Abcam, UK), mouse anti-CD11b (1:200, ab1211, Abcam, UK), rabbit anti-Arg-1 (1:200, #93668, CST, USA), rabbit anti-BrdU (1:200, orb10204, Biorbyt, UK), mouse anti-NeuN (1:1000, ab104224, Abcam, UK), rabbit anti-GFAP (1:1000, #12389, CST, USA), mouse anti-NF200 (1:1000, #2836, CST, USA), mouse anti-MAP2 (1:1000, 556320, BD Biosciences, USA), rabbit anti-5-HT (1:10000, S5545, Sigma, USA), rabbit anti-TH (1: 1000, ab112, Abcam, UK), and rabbit anti-Syn-1 (1:200, #5297, CST, USA).

27. Characterization of inflammatory cytokines

To evaluate the inflammation level of the focal spinal cords, pro- and anti-inflammatory cytokines were detected using an inflammatory PCR array (Wcgene® biotech, China) according to the manufacturer’s instructions. Briefly, fresh spinal cords (5 mm length) were removed from the lesion epicenter at 3 dpi. Total RNA was extracted from the spinal cords using TRIzol reagent, followed by reverse transcription. PCR array testing was carried out on a 480II

Real-Time PCR Detection System.

IL-1β, IL-6, IL-10, and TNF-α levels were measured using ELISA kits (Multi Sciences, China). 5 mm length of spinal cords at 3 dpi were lysed in protein lysis buffer, fragmentized by sonication, and centrifuged. Inflammatory cytokines in the supernatant was used for ELISA tests according to the protocols described by the manufacturer. The data were normalized by total protein levels of tissues.

28. Identification of microglia/macrophage phenotype

For flow cytometry measurements, spinal cord specimens (5 mm) were collected from SCI rats at 7 dpi. The tissues were incubated with collagenase IV and DNase for 30 min and mechanically separated by a 70 μm cell strainer to obtain a single cell suspension. After centrifugation at 300 *g* for 5 min, cells were incubated with antibodies for 15 min at 25 °C and fixed with MEDIUM A of the fix & perm kit (Multi Sciences, China) for 5 min. After centrifugation at 300 *g* for 5 min, precipitation was resuspended by MEDIUM B of the kit and incubated with intracellular antibodies for 15 min, followed by washing 3 times. Cells were analyzed by flow cytometry (BD Accuri™ C6 cytometry, USA). In the assay, samples were randomly selected from each group for detection (n=3). The following antibodies were used for staining: mouse anti-CD11b-APC (1:50, AR011BC05, Multi Sciences, China), mouse anti-CD206-PE (1:50, sc-58986, Santa Cruz, USA), and mouse anti-CD86-FITC (1:50, 200305, Biolegend, USA).

29. Statistical analysis

Quantitative data were reported as mean ± standard deviations (S.D.) and analyzed with GraphPad Prism software (version 7.0). Unpaired Student's t-test (two-tailed) was used for the mean comparison of two groups. One-way ANOVA followed by Tukey's post hoc analysis was used to compare the mean values of three groups and more. Data were analyzed by two-way ANOVA in the BBB scores matched at different time points. $P<0.05$ was determined to be statistically significant. All the experiments were performed with at least 3 replicates in each group.

Section 2. Figs. S1–S36 and Table S1

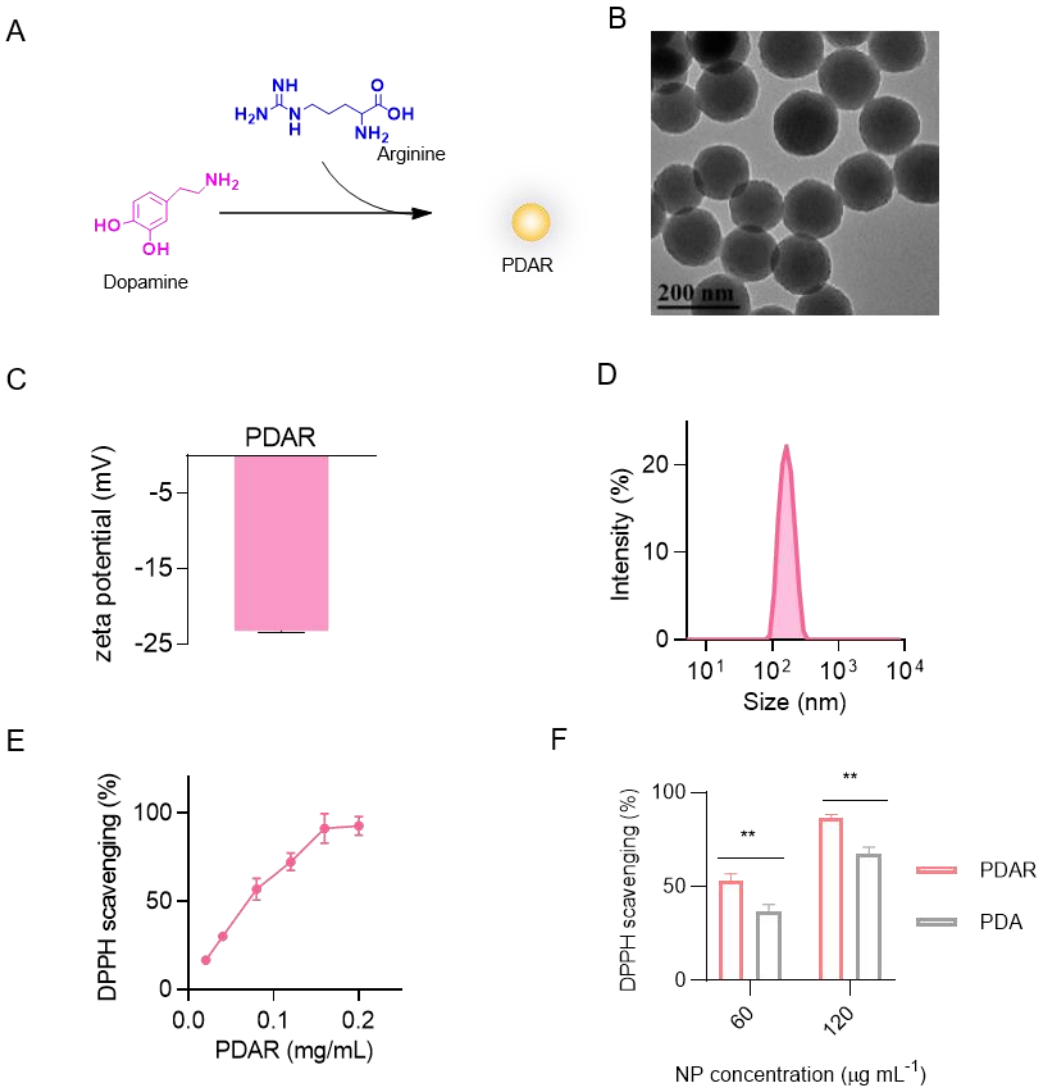

Fig. S1. (*A*) Scheme of the formation of PDAR NPs by polymerization of dopamine in the presence of arginine. (*B*–*E*) TEM image (*B*), ζ-potential (*C*), size distribution (*D*) and DPPH scavenging (*E*) of PDAR NPs. (*F*) DPPH scavenging of PDAR and PDA NPs.

PDAR NPs were synthesized via the polymerization of dopamine in the presence of arginine. The average diameter and ζ-potential of the PDAR NPs were 159.3 nm and –23.2 mV, respectively. The radical scavenging activity of the PDAR NPs was investigated using the DPPH assay, and was significantly higher than that of pure polydopamine NPs due to the incompact π-stacked nanostructures induced by arginine (1, 2).

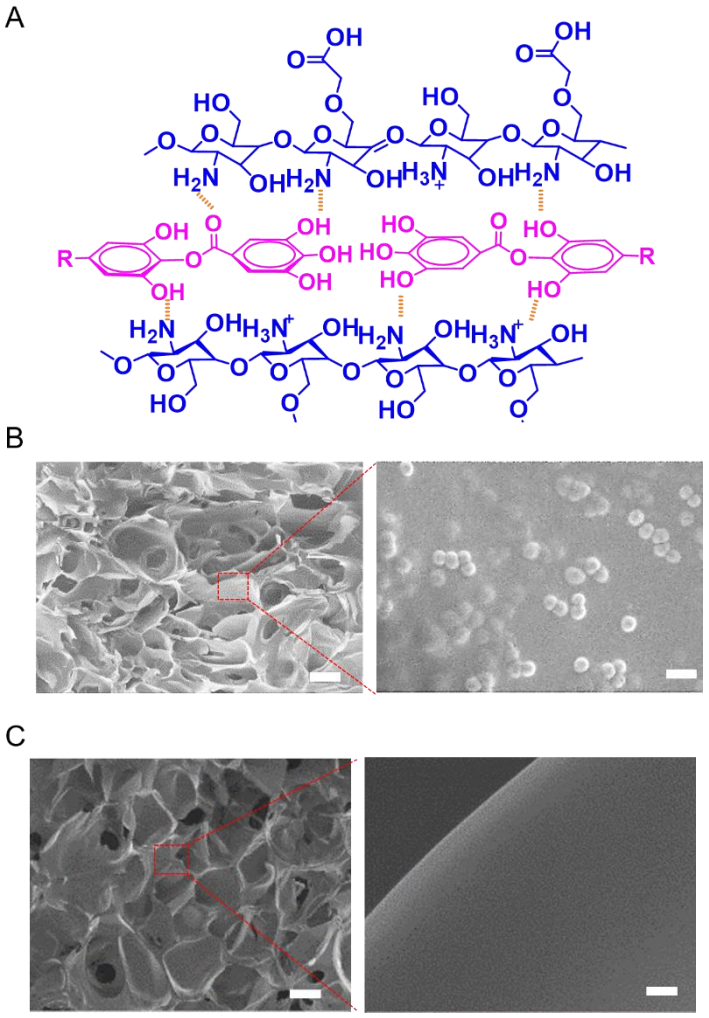

Fig. S2. (*A*) Scheme of the intermolecular interactions between CC and phenolic compounds. (*B* and *C*) SEM images of TPC (*B*) and TC (*C*) hydrogels. Scale bars: 50 μm (left) and 500 nm (right).

SEM showed that three-dimensional porous structures were observed in both TC and TPC hydrogels, and PDAR NPs were homogeneously distributed in the TPC hydrogels.

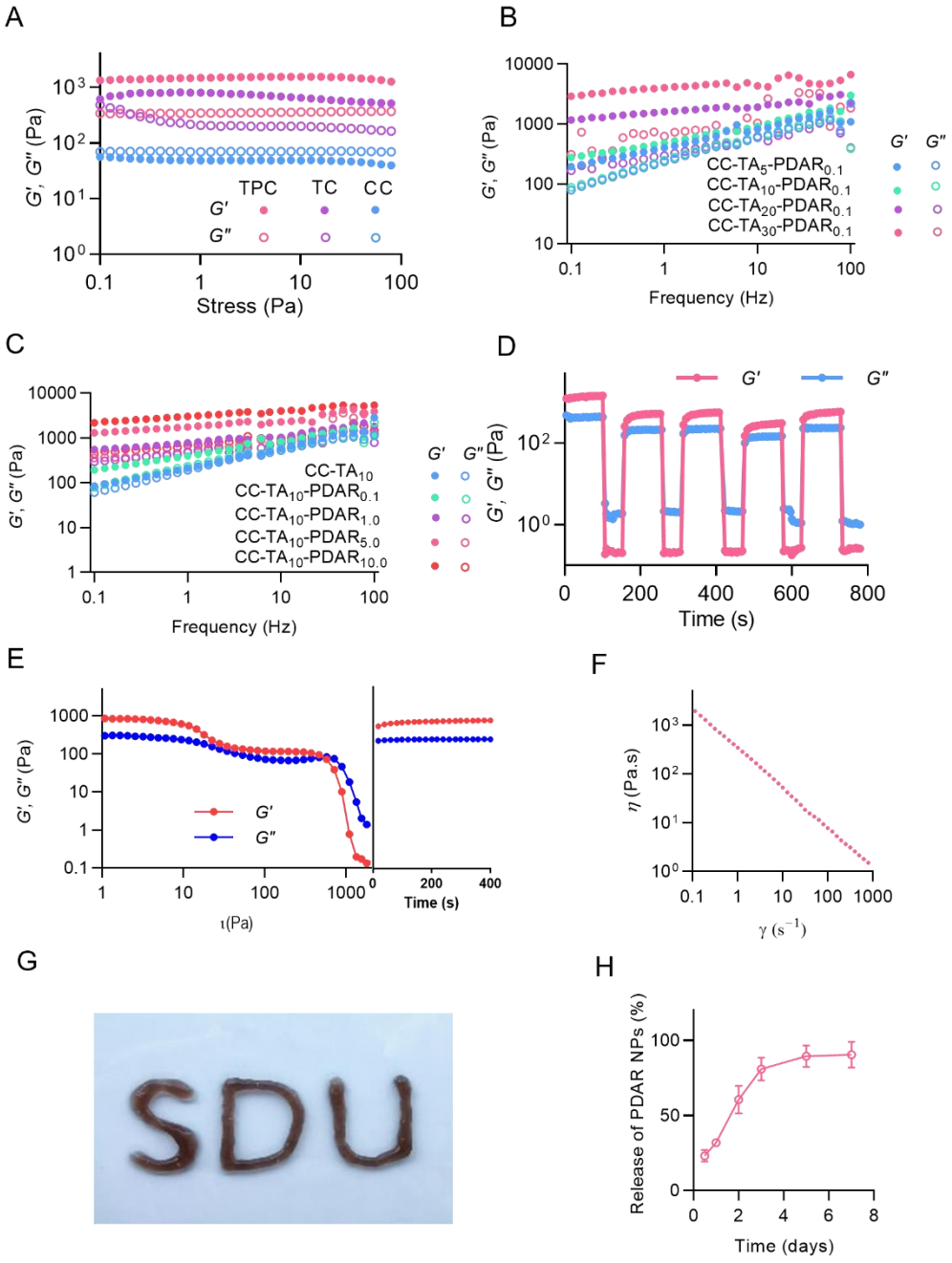

Fig. S3. (*A*) G′ and G″ of CC, TC and TPC versus shear stress. (*B* and *C*) *G′* and *G″* of the TPC hydrogels versus frequency. (*B*) CC and PDAR concentrations were fixed at 100 and 0.1 mg mL^{-1}, respectively. (*C*) CC and TA concentrations were fixed at 100 and 10 mg mL^{-1}, respectively. Frequency sweep was performed at a constant strain of 1% from 0.01 to 100 Hz at 25 °C. (*D*) Cyclic G′ and G″ of TPC hydrogels as a function of step stress from 1 Pa (interval of 100 s) to 1000 Pa (interval of 60 s). (*E*) Dynamic oscillatory rheology under the shear stress ranging from 0.1 to 1000 Pa. The time recovery dependence of the TPC hydrogels was 1 Hz. (*F*) Apparent viscosity (*η*) rheology of TPC hydrogels as a function of shear rate. (*G*) The words written with hydrogel strips extruded from a syringe. (*H*) Release rate of PDAR NPs from TPC hydrogels in PBS solutions.

Rheological studies revealed that the storage modulus (*G′*) was lower than loss modulus (*G″*) for the CS scaffolds, indicating a liquid-like behavior of the CC solution. By contrast, *G′* was higher than *G″* for TC and TPC hydrogels, which showed a typical characteristic of hydrogels (3). In addition, *G′* values of the hydrogels were positively correlated with TA or PDAR concentrations, which indicated that both TA and PDAR contributed to the mechanical properties of the resultant hydrogels. When a large shear force (1000 Pa) was applied on TPC hydrogels, liquid behavior of the hydrogel was observed, while the hydrogel recovered immediately when a low shear force (1 Pa) was applied. The repeatable recovery profiles of *G′* and *G″* indicated self-healing property of the hydrogels. The shear-thinning behavior of TPC hydrogels was presented by gradually reduced viscosity when the shear rate increased from 0.1 to 1000 s^{-1}. Thus, the hydrogels could be injectable and used as “ink” for writing. Moreover, the embedded PDAR NPs could be released from TPC hydrogels in PBS solutions.

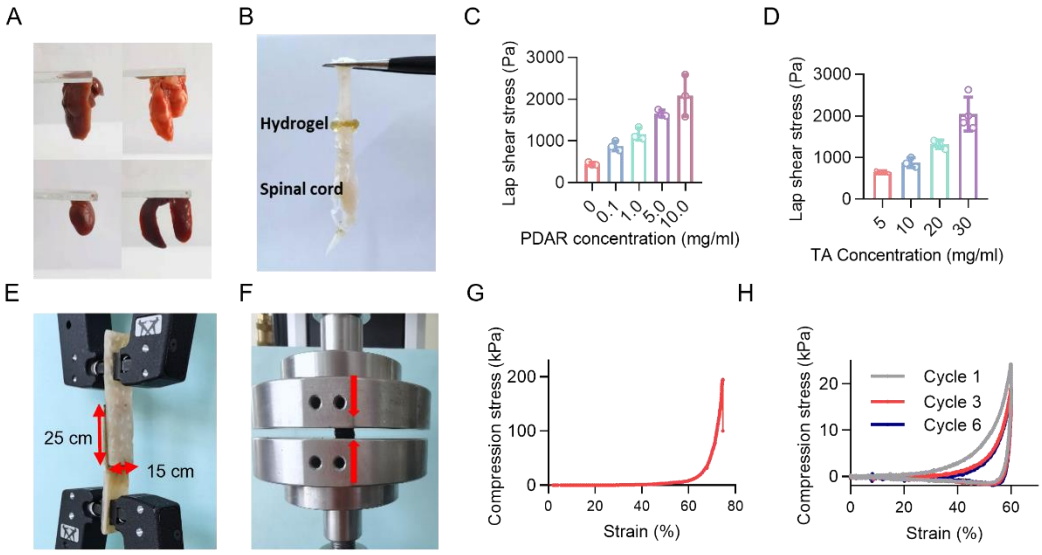

Fig. S4. (*A*) Photograph of the adhesion of TPC hydrogels to various organs. The tissue is hanging from the hydrogel, which is pasted on the glass on top. (*B*) Fractured spinal cords bridged by TPC hydrogels. (*C* and *D*) Measured lap shear stress of TPC hydrogels as a function of the concentration of PDAR (*C*) and TA (*D*). (*E* and *F*) Digital photos showing the setup of adhesion force test (*E*) and compression force test (*F*). (*G*) Typical compression stress-strain curve of TPC hydrogels. (*H*) Cyclic compressive test of TPC hydrogels with the strain fixed at 60%.

Both TC and TPC hydrogels possessed tissue adhesive capacities, which benefited from the native adhesive property of phenolic compounds (4, 5). In particular, separate spinal cords were bridged using TPC hydrogels. The adhesion strength of the TPC increased with an increase in the concentrations of TA and PDAR NPs. Also, TPC hydrogels could withstand a high compression strain of 75% without breaking. After removing the compression force, the hydrogels were able to recover.

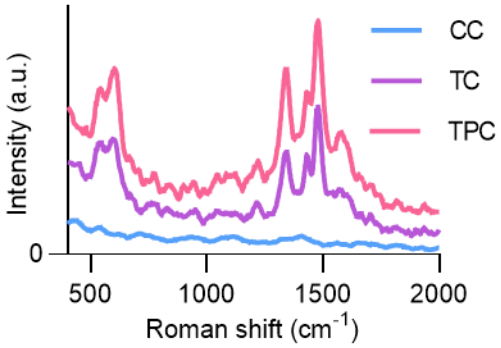

Fig. S5. Raman spectra of CC, TC and TPC hydrogels.

Resonance Raman spectroscopy was performed to detect the adsorption of Fe in the TC and TPC hydrogels. The bands at 650~500 cm^{-1} and 1600~1200 cm^{-1} were attributed to the Fe–O vibration due to the metal–phenolic coordination and phenolic ring vibrations, respectively (6, 7).

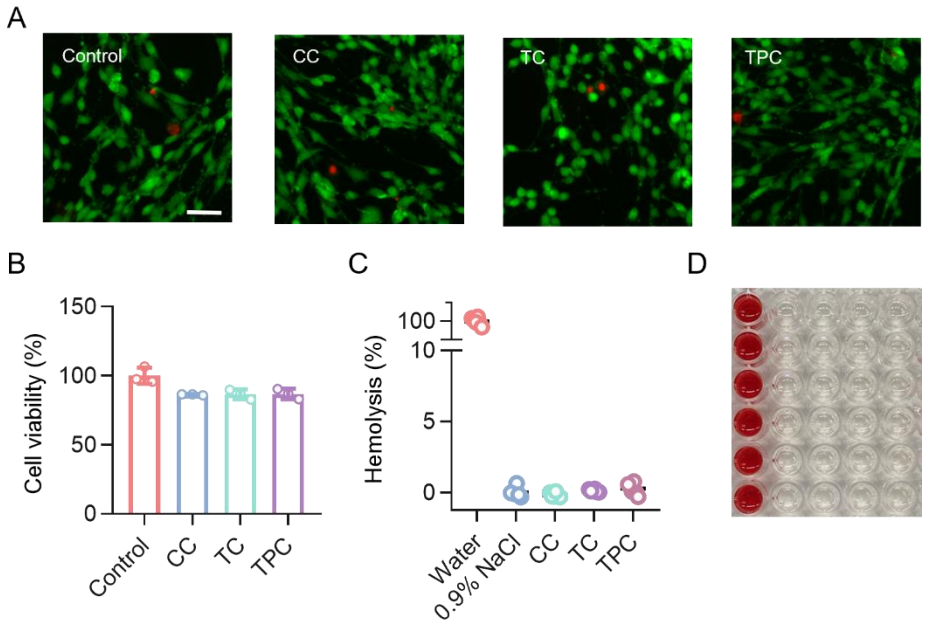

Fig. S6. (*A*) Live (green)/dead (red) viability assay of PC12 cells after incubation with 20 μL PBS (control) or different materials for 24 h. (*B*) Cytotoxicity of CC, TC, and TPC hydrogels against PC12 cells after incubation for 24 h (n = 3). (C and D) Hemolytic ratios (*C*) and photographs (*D*) of hemolytic activity assay. The wells (six wells per column) from left to right represent water (positive control), 0.9% NaCl (negative control), CC, TC, and TPC hydrogel (n = 6). All data represent the mean ± SD. Cytocompatibility and hemocompatibility tests revealed that the hydrogels showed negligible toxicity and hemolytic activity.

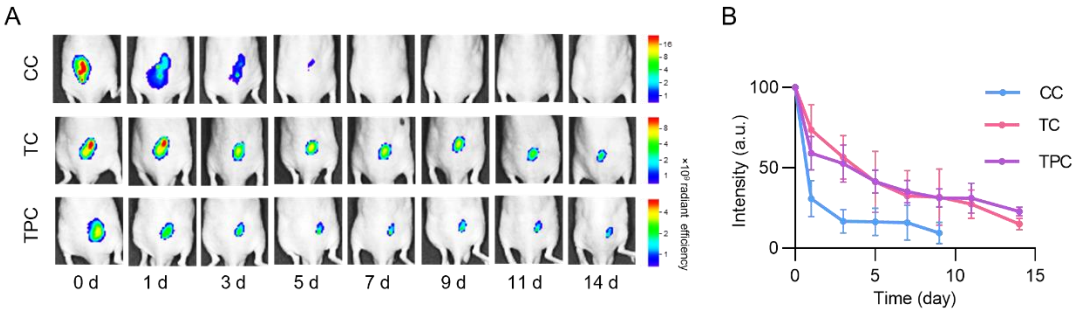

Fig. S7. (*A* and *B*) Real-time *in vivo* images (*A*) and fluorescence analysis (*B*) of the residual CC, TC and TPC in animals after subcutaneous injection.

To track the *in vivo* biodegradation of the hydrogels, FITC-labelled CC was used to prepare the hydrogels followed by subcutaneous injection. The fluorescence of the TC and TPC hydrogels was ~20% on day 14, while 90% of the CC scaffolds were degraded within 5 days.

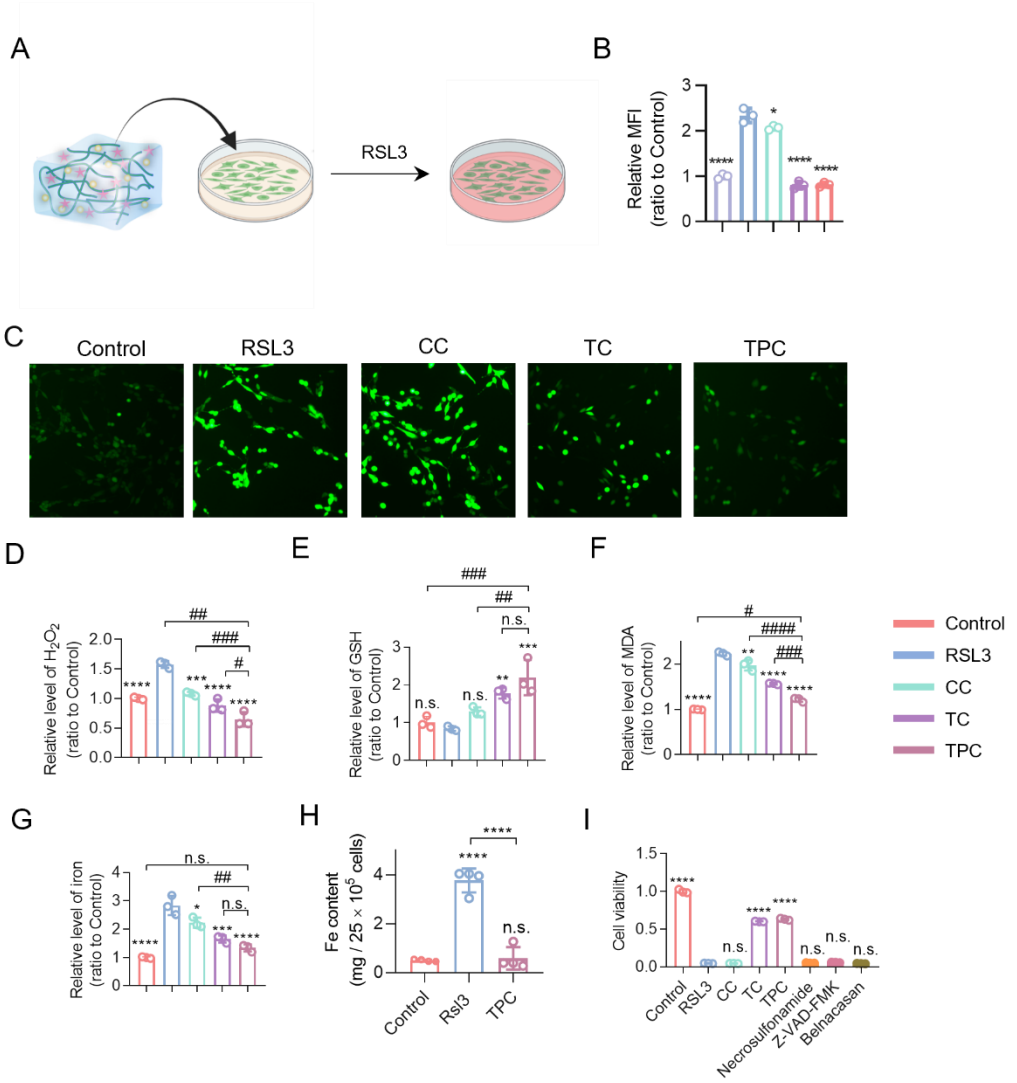

Fig. S8. (*A*) Scheme of ferroptosis induced by RSL3. (*B* and *C*) Flow cytometry analysis (*B*) and representative fluorescence images (*C*) of PC12 cells after the stimulation of RSL3 and subsequent treatment with different materials for 12 h, showing intracellular ROS level of using DCFH-DA assay. (*D*–*G*) Statistical analysis of relative levels of H_2O_2 (n = 3) (*D*), GSH (n = 3) (*E*), MDA (n = 3) (*F*), and iron ions (n = 3) (*G*). (*H*) Fe contents of cells in Control, Rsl3 and TPC groups according to ICP-MS. (*I*) Cell viability of PC12 cells incubated with RSL3 and different materials (n = 3). Necrosulfonamide, Z-VAD-FMK and Belnacasan are necrosis, pyroptosis and apoptosis inhibitors, respecitovely. All data are mean ± SD. One-way ANOVA followed by Tukey's post hoc test (*D*–*H*). $^{*}p < 0.05$, $^{**}p < 0.01$, $^{***}p < 0.001$, and $^{****}p < 0.0001$ compared with the RSL3 group. $^{\#}p < 0.05$, $^{\#\#}p < 0.01$, $^{\#\#\#}p < 0.001$, and $^{\#\#\#\#}p < 0.0001$ compared with the TPC group. n.s. = not significant.

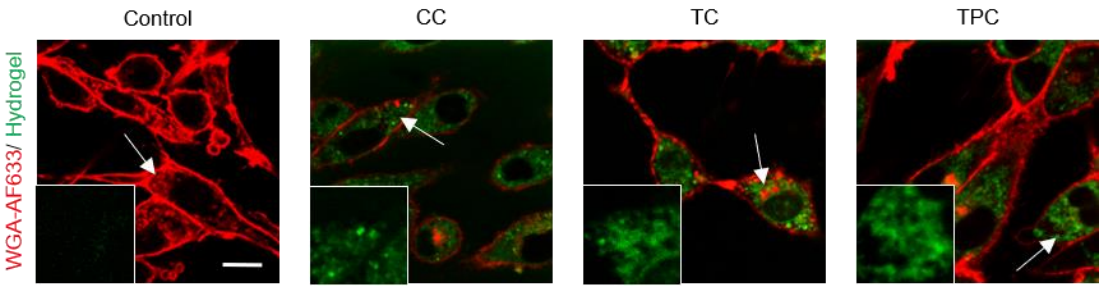

Fig. S9. CLSM images of PC12 cells after incubation with FITC-labelled CC, TC (FITC-labelled CC), and TPC (FITC-labelled CC) for 24 h. Cell membranes were stained with WGA-AF633 (red). Scale bar is 10 μm. Enlarged images of the box region correspond to the pointing of arrows.

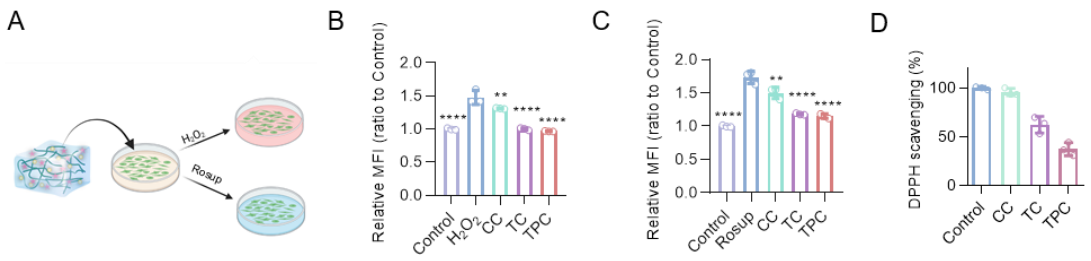

Fig. S10. (*A*) Scheme of antioxidant experiment. (*B* and *C*) Flow cytometry analysis of PC12 cells after incubation with H_2O_2 (B), and Rosup (*C*) in the presence of different materials for 12 h, showing intracellular ROS level. (*D*) *In vitro* DPPH scavenging of CC, TC, and TPC hydrogels.

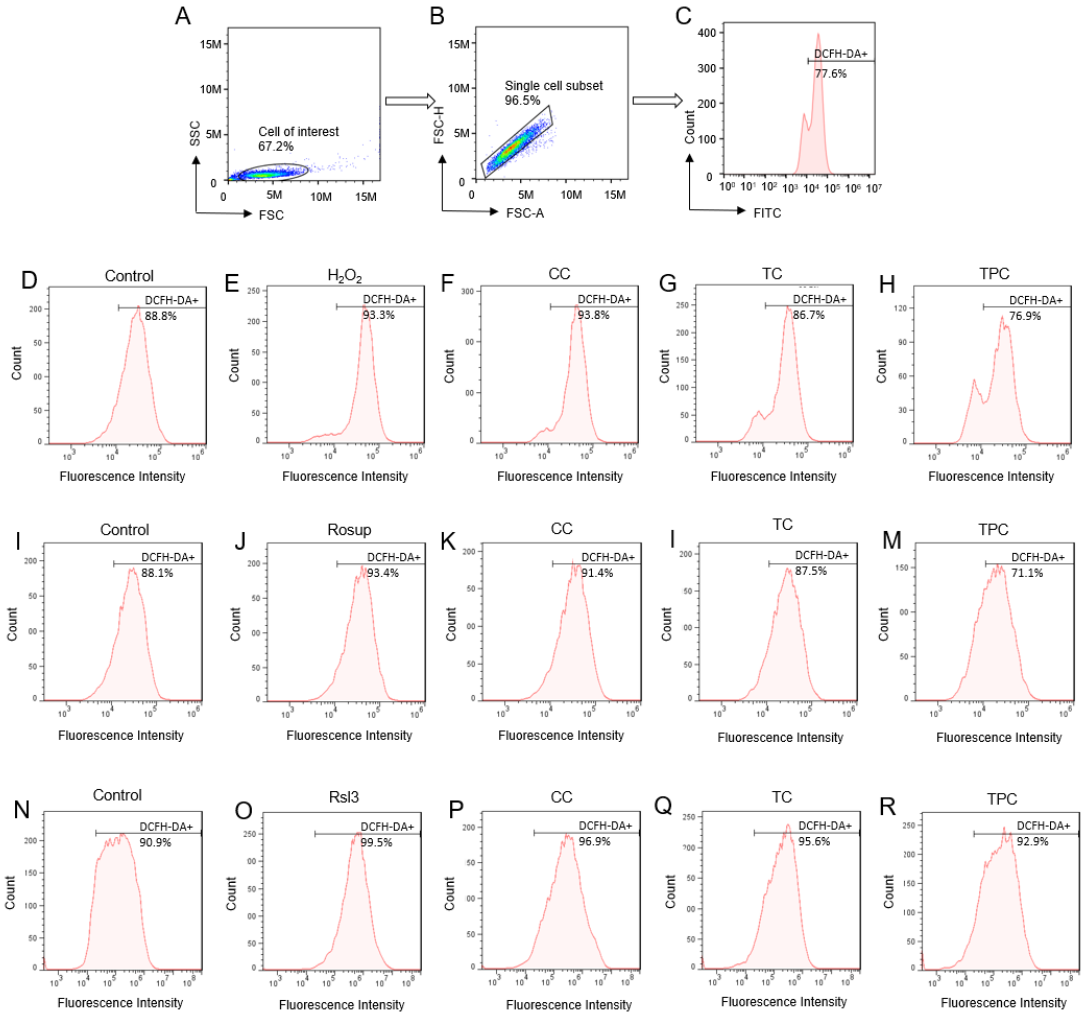

Fig. S11. (*A*–*C*) Sequential gating of *SI Appendix*, Figs. S8*B*, S10 *B* and *C*. The proportion of DCFH-DA$^+$ cells represent the groups after incubation with (*D*–*H*) H_2O_2, (*I*–*M*) Rosup, and (*N*–I) RSL3 in the presence of different materials for 12 h.

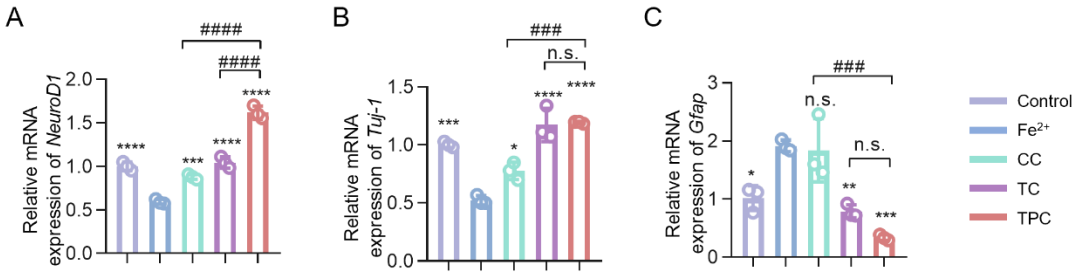

Fig. S12. (*A*–*C*) Relative mRNA expression of *Neurod1* (*A*), *Tuj1* (*B*) and *Gfap* (*C*) in NSPCs after the treatment of PBS (control), Fe^{2+}, CC, TC, and TPC for 7 days in differentiation medium (n = 3), which were normalized against control group. All data represent the mean ± SD. One-way ANOVA followed by Tukey's post hoc test. $^{*}p < 0.05$, $^{**}p < 0.01$, $^{***}p < 0.001$ and $^{****}p < 0.0001$ compared with Fe^{2+} group. $^{\#\#\#}p < 0.001$ and $^{\#\#\#\#}p < 0.0001$ compared with TPC. n.s. = not significant.

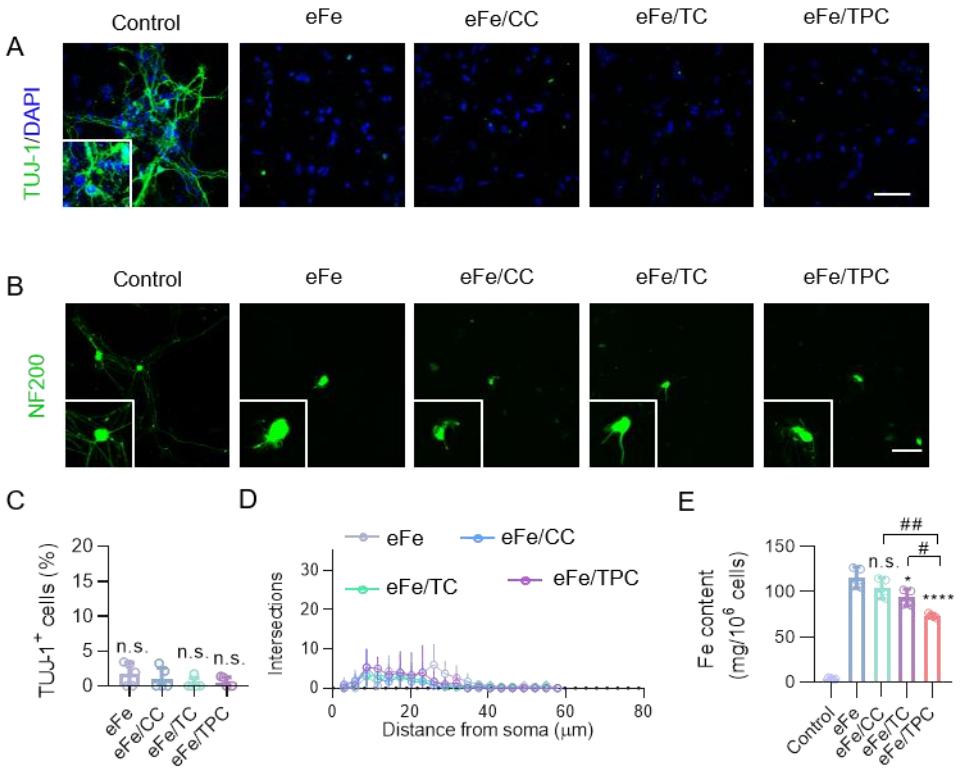

Fig. S13. (*A*) Representative fluorescence images of NSPC-derived cells in different groups at day 3, which were stained with anti-TUJ-1 antibodies (green), and DAPI (blue), respectively. Scale bar: 50 μm. (*B*) Representative fluorescence images of cultured DRG neurons, which were stained with anti-NF200 antibodies (green), and DAPI (blue). Scale bar: 50 μm. (*C*) Quantification of the percentages of TUJ-1$^+$ cells derived from NSPCs. (*D*) Sholl analysis of neurite outgrowth in DRGs incubated with different materials. (*E*) Fe contents in spinal cords of different groups according to ICP-MS. All data represent the mean ± SD. (*C* and *E*) One-way ANOVA followed by Tukey's post hoc test. $^{****}p < 0.0001$ compared with the eFe (*C*) or Control (*E*) groups. $^{\#}p < 0.05$ and $^{\#\#}p < 0.01$ compared with the eFe group. n.s. = not significant.

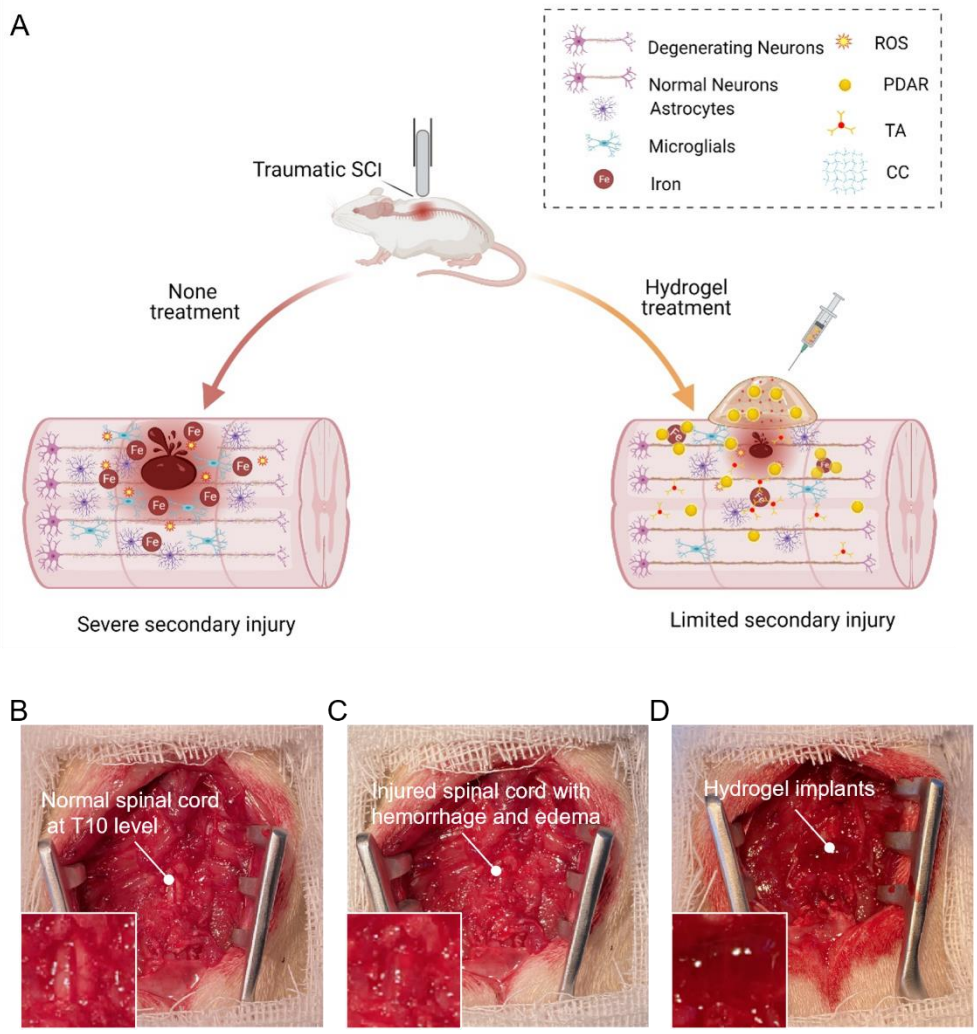

Fig. S14. (*A*) Scheme of the spinal cord injury and hydrogel treatment. (*B–D*) Photographs of normal spinal cord (*B*), injured spinal cord (*C*), and hydrogel implantation (*D*) at the injury site.

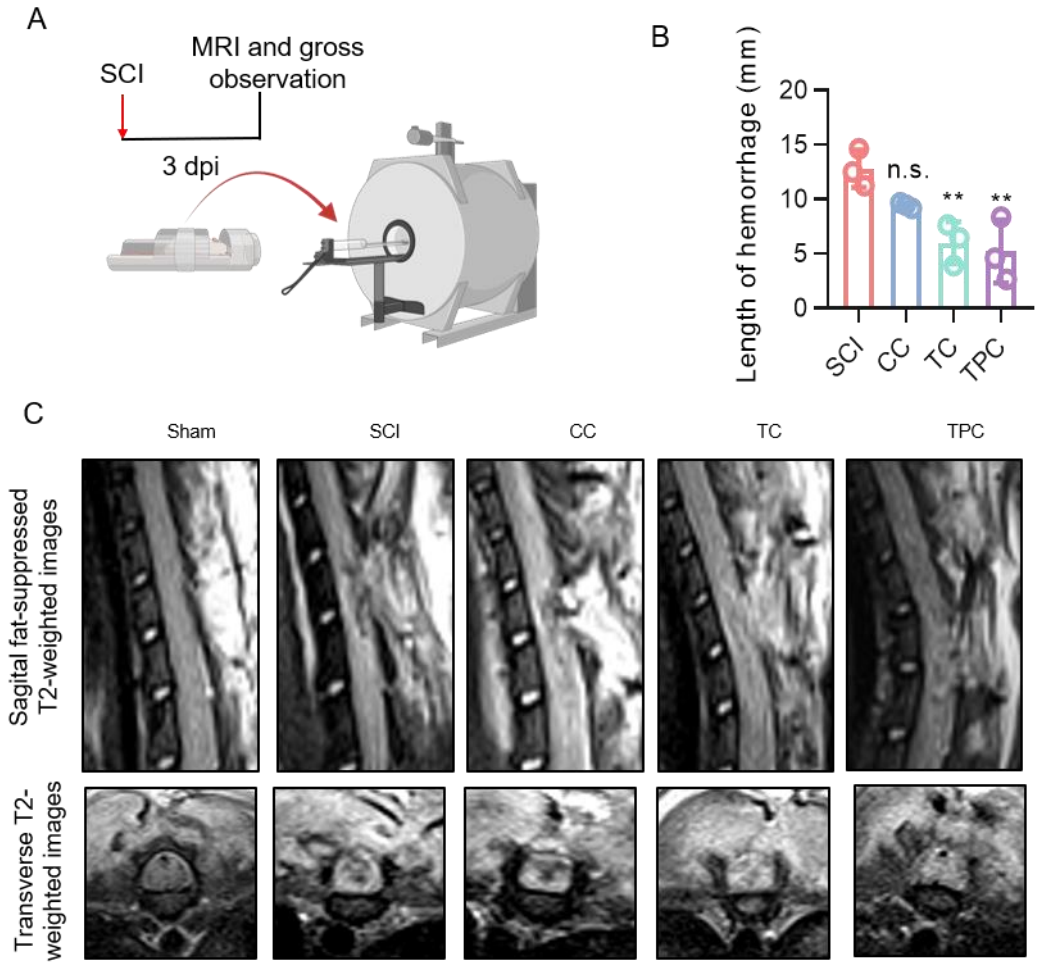

Fig. S15. (*A*) Experimental design of MRI. (*B*) The length of hemorrhage according to MRI images (n = 3). (*C*) Sagital fat-suppressed and transverse T2-weighted MRI images of spinal cords.

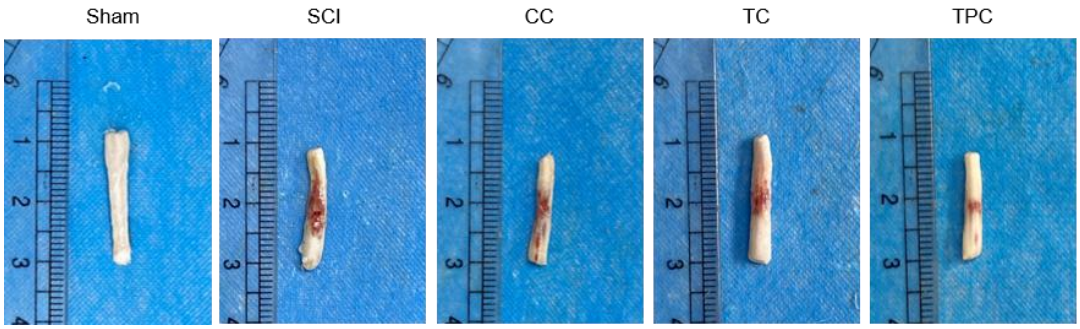

Fig. S16. Photographs of the spinal cords at 3 dpi in the different groups.

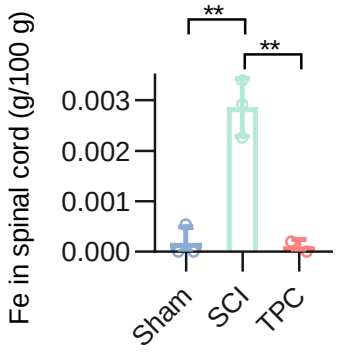

Fig. S17. Fe contents in spinal cord tissue of Sham, SCI and TPC groups according to ICP-MS. All data represent the mean ± SD. $^{**}p < 0.01$ compared with SCI group.

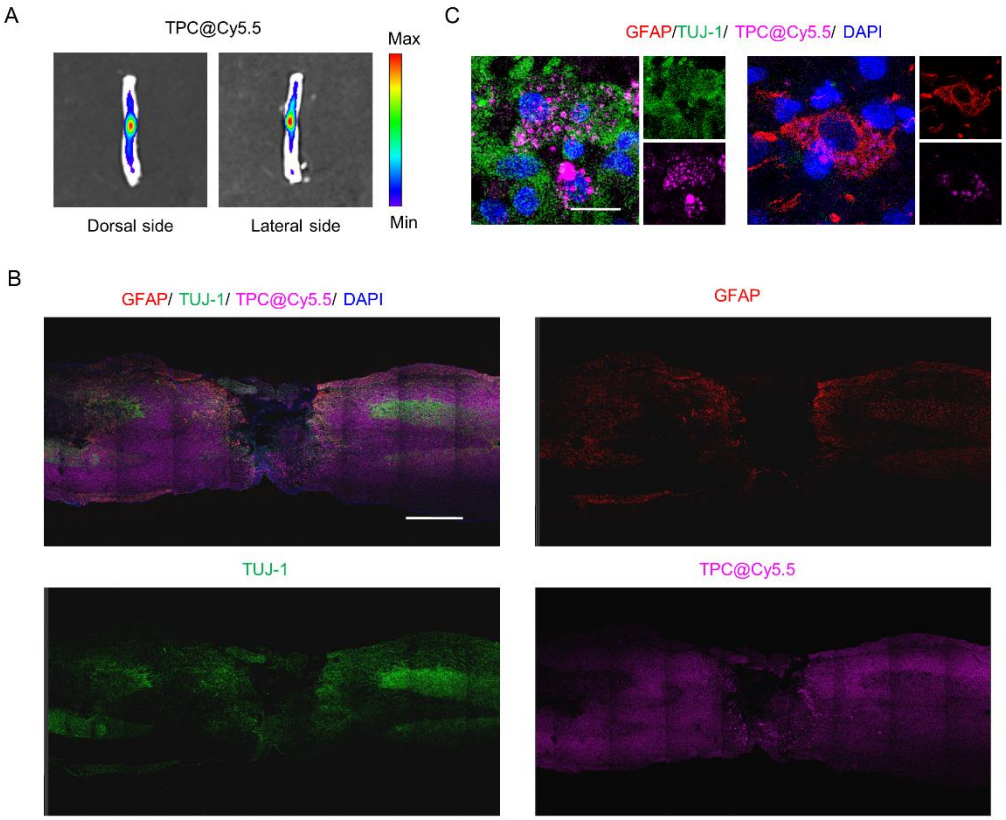

Fig. S18. (*A*) Representative fluorescent images of spinal cords after SCI at 3 dpi. (*B*, *C*) Representative longitudinal images (*B*) and enlarged images (*C*) of tissues from the Cy5.5-labelled TPC hydrogel (magenta)-treated spinal cords stained with anti-GFAP antibody (red) and anti-TUJ-1 antibody (green) and DAPI (blue). Scale bars: 500 μm (*B*) and 15 μm (*C*).

The fluorescence intensity of Cy5.5-labelled TPC (TPC-Cy5.5) hydrogels was considerably strong at the lesions of spinal cords. To further identify the hydrogels from immunofluorescence staining images, longitudinal spinal cord sections were analyzed. We found that TPC-Cy5.5 were colocalized with both TUJ-1+ neurons and GFAP+ astrocytes, suggesting that polyphenol-based hydrogels can penetrate into the injured spinal cords to regulate the microenvironments.

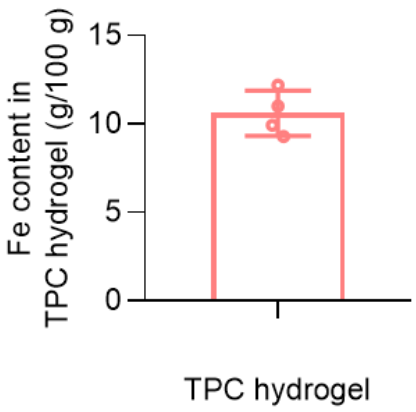

Fig. S19. (*A*) Fe contents in TPC hydrogels at 7 dpi according to ICP-MS.

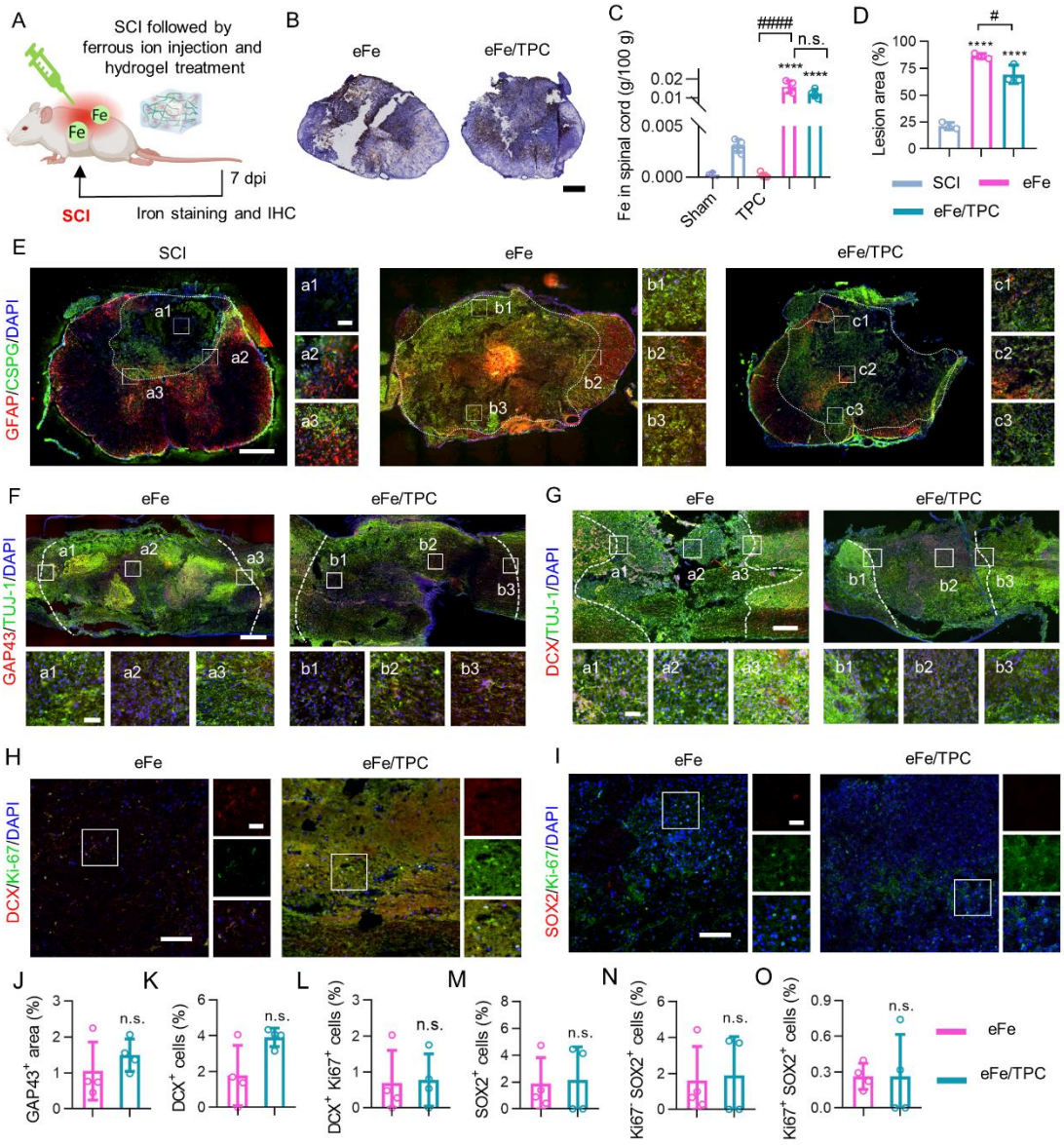

Fig. S20. Effect of hydrogels on iron dyshomeostasis after SCI. (*A*) Experimental design of iron dyshomeostasis after SCI. (*B*) Representative images of the transverse sections of spinal cord lesions at 7 dpi. Iron ions (brown) were stained with DAB-enhanced Prussian blue. Scale bar: 500 μm. (*C*) Iron contents in spinal cords measured by ICP-MS. (*D*) Quantification of lesion areas of different groups in (*E*). (*E*) Representative immunofluorescence staining images of the transverse spinal cord sections stained with anti-GFAP (red), anti-CSPG antibodies (green), and DAPI (blue). Scale bars: 500 μm. Enlarged images of the box regions are shown in the right panels. Scale bars: 50 μm. (*F*, *G*, *H* and *I*) Representative immunofluorescence staining images of lesion areas at 7 dpi stained with antibodies against GAP43 (red)/TUJ-1 (green)/DAPI (blue) (*F*), DCX (red)/TUJ-1 (green)/DAPI (blue) (*G*), DCX (red)/Ki-67 (green)/DAPI (blue) (*H*), SOX2 (red)/Ki-67 (green)/DAPI (blue) (*I*), respectively. Scale bars: 500 μm (*F* and *G*) and 50 μm (*H* and *I*). Enlarged images of the box regions are shown in the bottom (*F* and *G*) or right (*H* and *I*) panels. Scale bar: 50 μm (*F* and *G*) and 10 μm (*H* and *I*). (*J*–*O*) Quantification of the percentage of GAP43^{+} area (*J*), DCX^{+} (*K*), DCX^{+} Ki67^{+} (*L*), SOX2^{+} (*M*), Ki67^{-} SOX2+ (*N*), and Ki67^{+} SOX2^{+} (*O*) cells in the focal areas. All data represent the mean ±

SD. (*C* and *D*) One-way ANOVA followed by Tukey's post hoc test; (*J*–*O*) Student's two-tailed unpaired t-test. $^{****}p < 0.0001$ compared with the SCI groups. $^{\#}p < 0.05$ and $^{\#\#\#\#}p < 0.0001$ compared with the eFe group. n.s. = not significant.

The Fe contents in spinal cords (100 g) were ~0.2, 2.8, 0.3, 15.3 and 12.3 mg in the Sham, SCI, TPC, eFe and eFe/TPC groups according to ICP-MS, respectively. The eFe and eFe/TPC groups resulted in larger lesion areas, which was approximately 4 and 3.5 times larger than that of the SCI group, respectively. Moreover, a large number of astrocyte activation and glial scar formation were observed in SCI, eFe and eFe/TPC groups) There were no significant differences in $GAP43^{+}$ newborn fibers, DCX^{+} neuroblasts, $SOX2^{+}$ stem cells between eFe and eFe/TPC groups. These results suggest that exceeded ion accumulation induces severe neural regenerative disorders, which cannot be rescued by TPC hydrogels. The reason is that iron ions surpassed the chelation ability of TPC hydrogels, which results in the disordered iron homeostasis and therefore tissue inflammation and neuronal impairment.

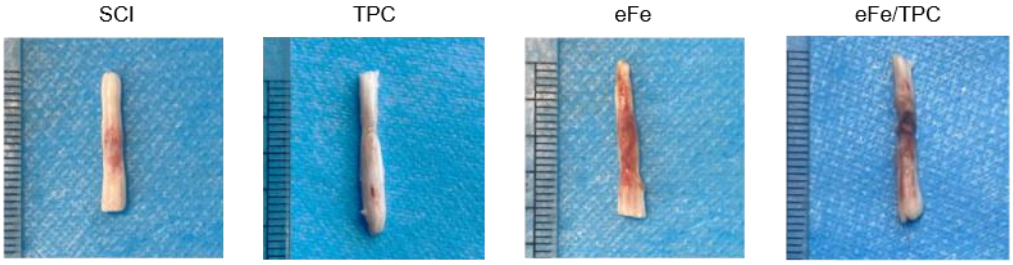

Fig. S21. Photographs of the spinal cords in the different groups at 7 dpi.

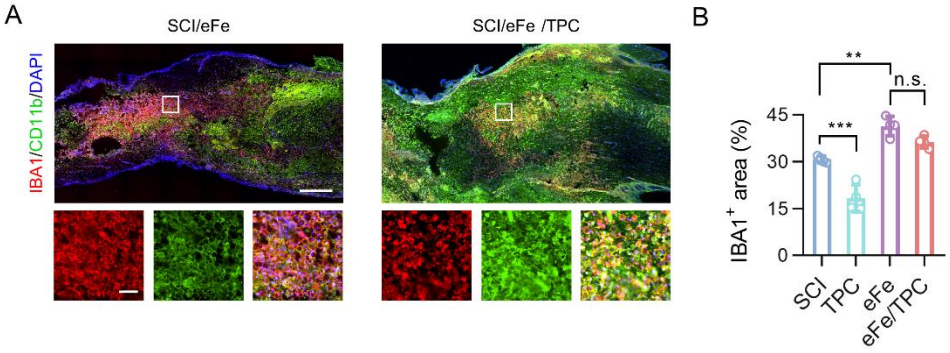

Fig. S22. (*A*) Representative images of lesion areas in different groups at 7 dpi, which were stained with anti-IBA1 (red)/anti-CD11b antibodies (green)/DAPI (blue). Enlarged images of the box regions are shown in the bottom panel. Scale bars: 500 μm (top) and 50 μm (bottom). (*B*) Quantification of lesion areas of different groups based on (*A*). All data represent the mean ± SD. One-way ANOVA followed by Tukey's post hoc test. **p < 0.01, and ***p < 0.001. n.s. = not significant.

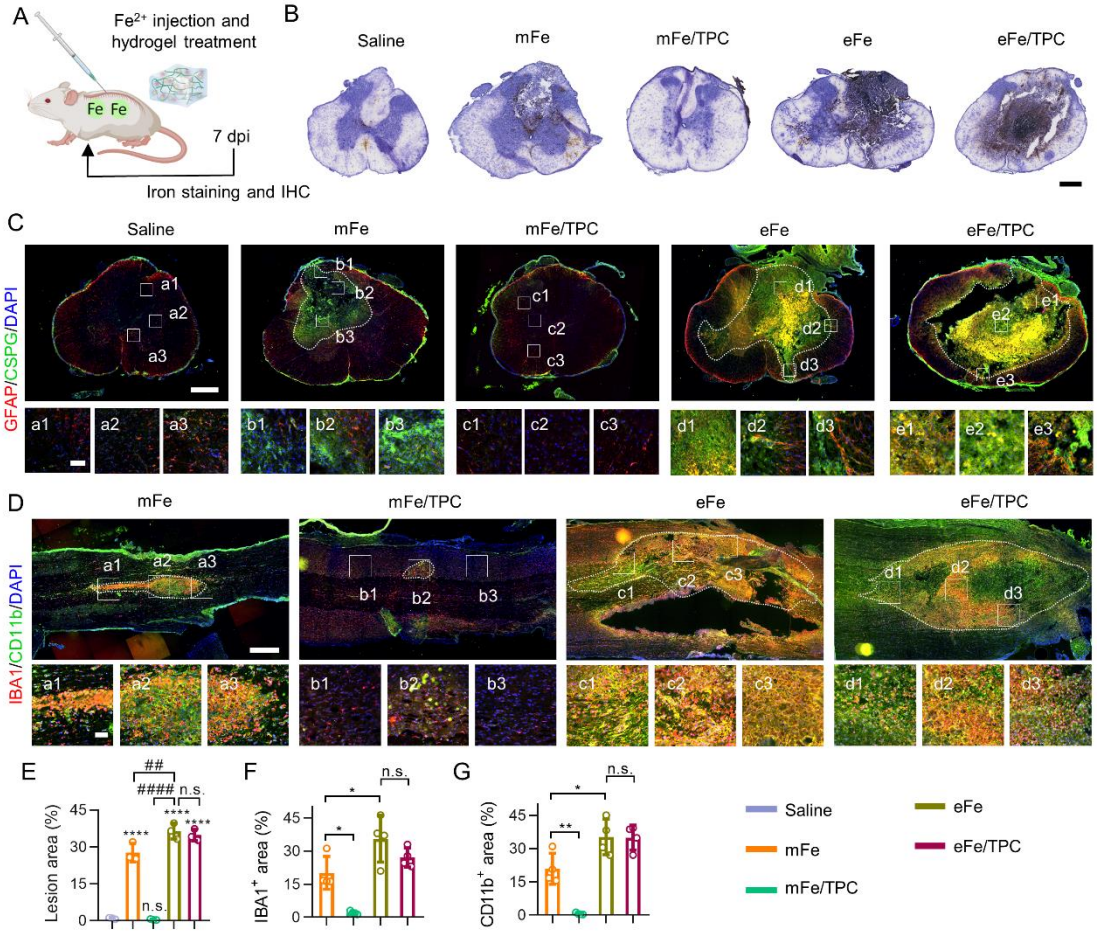

Fig. S23. Effect of hydrogels on iron-overloaded normal spinal cords. (A) Experimental design of iron overloading on normal spinal cords. (B) Representative images of the transverse sections of spinal cord lesions at 7 dpi. Iron ions (brown) were stained with DAB-enhanced Prussian blue. Scale bar: 500 μm. (C) Representative immunofluorescence staining images of the transverse spinal cord sections stained with anti-GFAP (red), anti-CSPG antibodies (green), and DAPI (blue). Scale bars: 500 μm. Enlarged images of the box regions are shown in the bottom panel. Scale bars: 50 μm. (D) Representative images of lesion areas in different groups at 7 dpi, which were stained with anti-IBA1 (red)/anti-CD11b antibodies (green)/DAPI (blue). Scale bars: 500 μm. Enlarged images of the box regions are shown in the bottom panel. Scale bars: 50 μm. (F) Quantification of lesion areas of different groups in (C). Quantification of the percentage of IBA1$^+$ area (F), CD11b$^+$area (G) in the focal sites in (D). All data represent the mean ± SD. (E, F and G) One-way ANOVA followed by Tukey's post hoc test. *$p < 0.05$, **$p < 0.01$, and ****$p < 0.0001$. $^{\#}p < 0.05$, $^{\#\#}p < 0.01$, and $^{\#\#\#\#}p < 0.0001$. n.s. = not significant.

Normal spinal cords were damaged by excess iron ions, resulting in a large number of activated GFAP+ astrocytes and CSPG signals of glial scars in the eFe and eFe/TPC groups. In addition, the lesion area of the eFe group (36.4 ± 3.2%) was significantly larger than that of the mFe group (27.6 ± 3.8%), indicating excess ferrous ions were more disruptive to normal spinal cords. TPC hydrogels only were able to restore the damage induced by mFe instead of eFe. A large number of IBA-1$^+$ microglia cells and CD11b$^+$ macrophages were distributed around the lesion

in the mFe, eFe and eFe/TPC groups, while the mFe/TPC groups showed negligible recruitment of $IBA1^+$ and $CD11b^+$ cells.

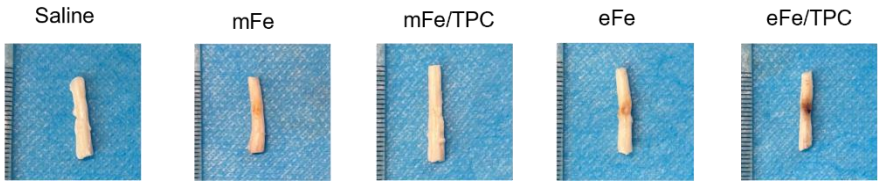

Fig. S24. Photographs of the spinal cords in the different groups at 7 dpi.

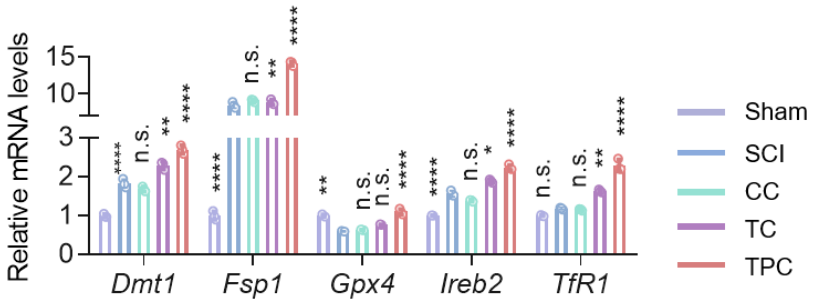

Fig. S25. *Dmt1*, *Fsp1*, *Gpx4*, *Ireb2*, and *TfR1* mRNA levels of the spinal cords at 3 dpi, which were normalized against the sham group (n = 3). All data represent the mean ± SD. One-way ANOVA followed by Tukey's post hoc test. $^{**}p < 0.01$, and $^{****}p < 0.0001$ compared with SCI group.

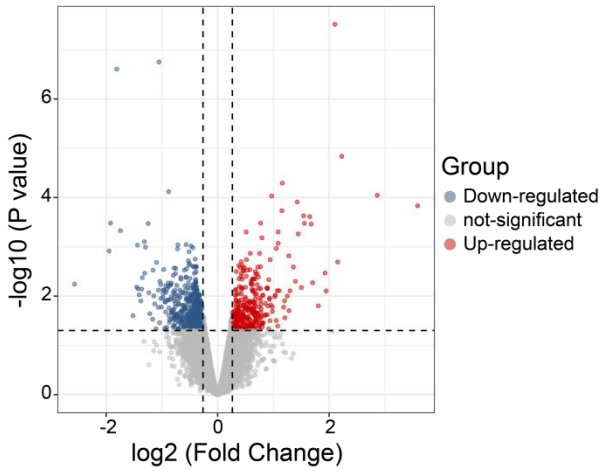

Fig. S26. Volcano plot of mRNA sequencing. Blue dots, gray dots, and red dots represent down-regulated, not-significant, and up-regulated genes, respectively.

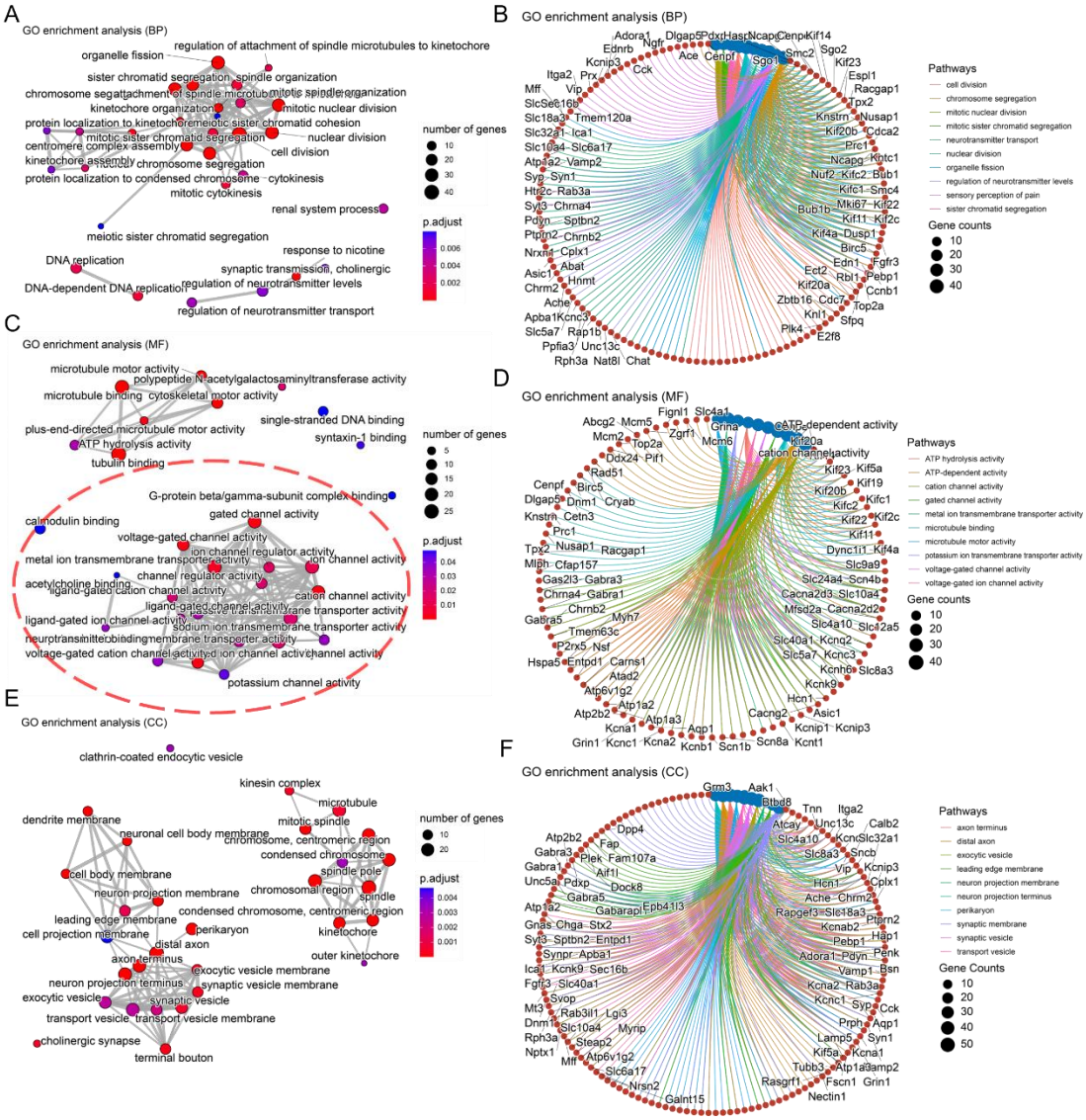

Fig. S27. (*A*–*F*) Enrichment map (*A*, *C*, *E*) and Gene-concept network (*B*, *D*, *F*) of biological processes, molecular function, and cellular components via GO analysis. The size of dots represents the number of enriched genes. The adjusted p-value is reflected on the red and blue bars. In the Gene-concept network, blue and red dots represent different enriched pathways and different enriched gene names, respectively, which are connected with corresponding colorful lines.

A

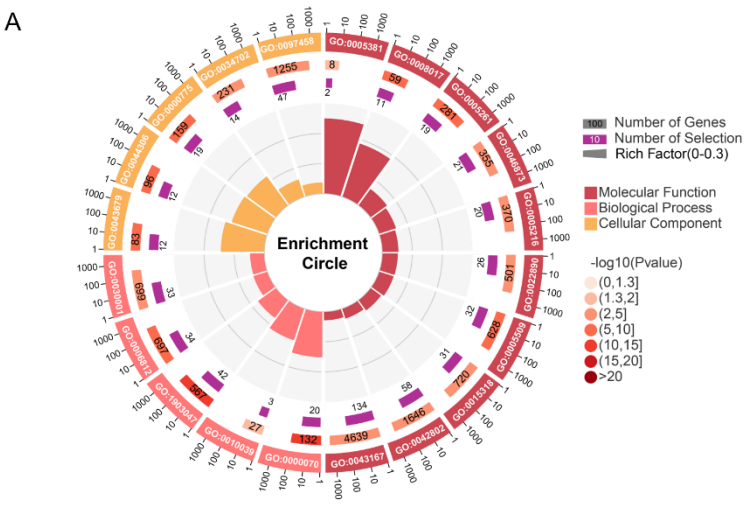

B

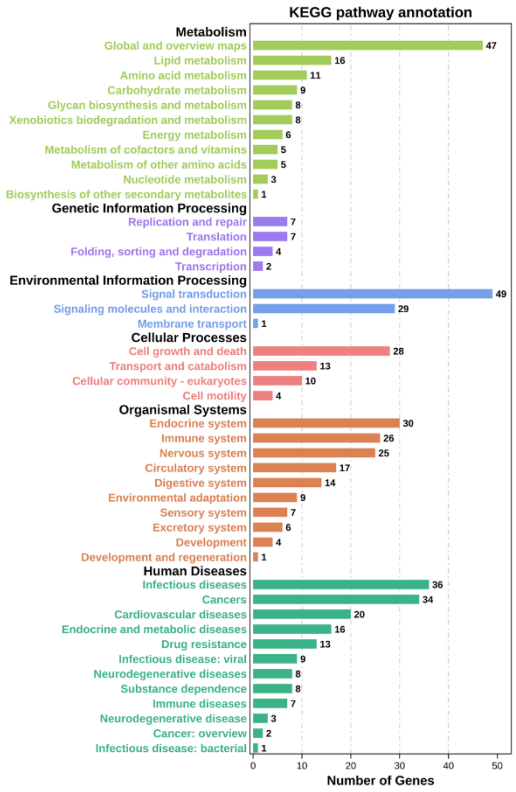

C

GO ID	Description
GO:0005381	iron ion transmembrane transporter activity
GO:0008017	microtubule motor activity
GO:0005261	cation channel activity
GO:0046873	metal ion transmembrane transporter activity
GO:0005216	ion channel activity
GO:0022890	inorganic cation transmembrane transporter activity
GO:0005509	calcium ion binding
GO:0015318	inorganic molecular entity transmembrane transporter activity
GO:0042802	identical protein binding
GO:0043167	ion binding
GO:0000070	mitotic sister chromatid segregation
GO:0010039	response to iron ion
GO:1903047	mitotic cell cycle process
GO:0006812	cation transmembrane transport
GO:0030001	metal ion transport
GO:0043679	axon terminus
GO:0044306	neuron projection terminus
GO:0000775	chromosome, centromeric region
GO:0034702	ion channel complex
GO:0097458	neuron part

Fig. S28. (*A* and *C*) Enrichment circle of GO analysis (*A*) and its description (*C*). (*B*) KEGG pathway analysis, mainly categorized as metabolism, genetic information processing, environmental information processing, cellular processes, organismal systems, and human diseases. The outermost circle represents the ID of the pathways. The second layer of the circle represents the number of all genes in a certain pathway. The third layer of the circle represents the number of DEGs in a certain pathway. The innermost layer of the circle represents the rich factor of a certain pathway.

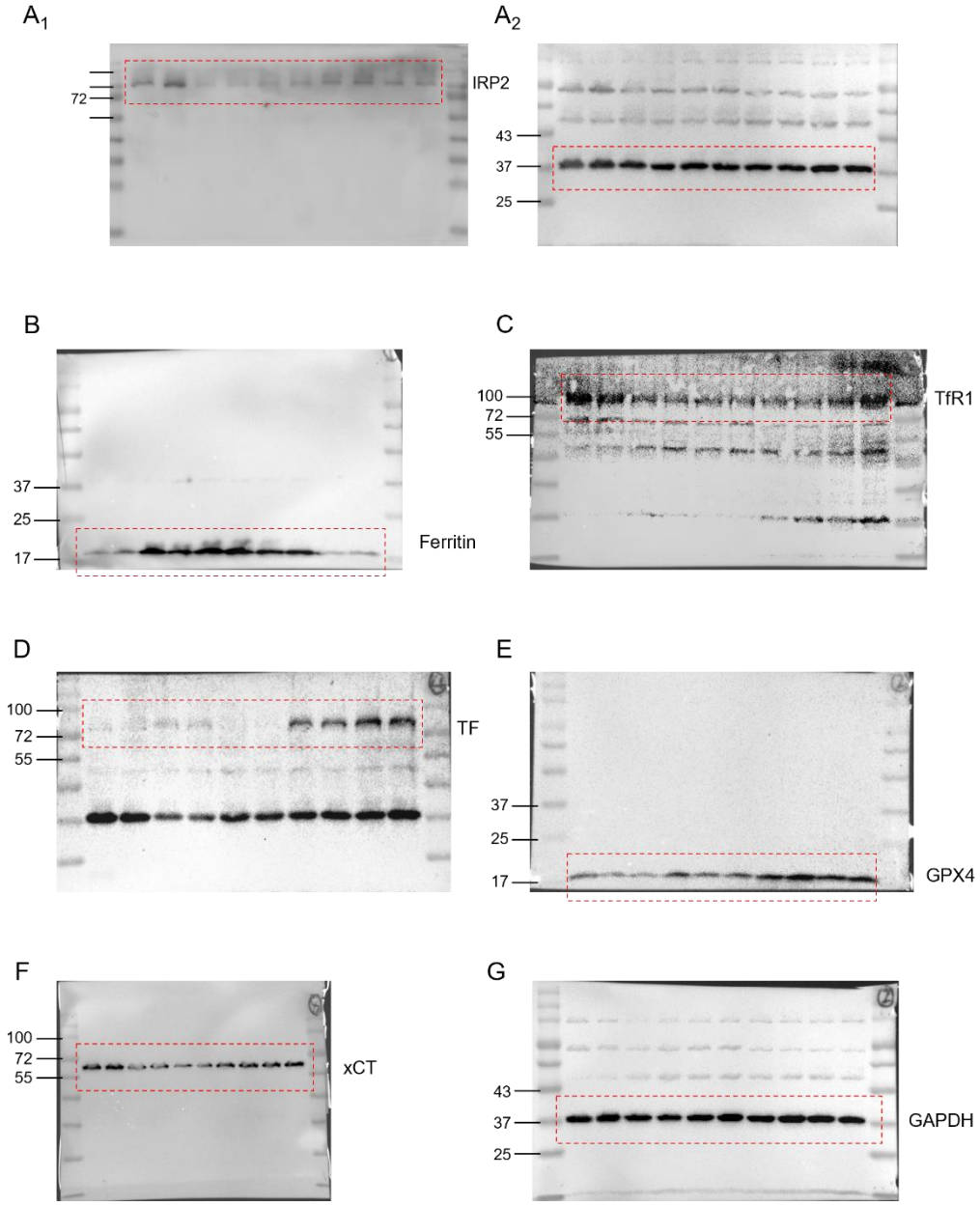

Fig. S29. Relevant areas of cropped blots in the Fig. 3*G* are shown with a dashed box in red. (*A*) Original blots of IRP2 (*A*1) and GAPDH (*A*2), which were from a same membrane with different exposure time to avoid overexposure of certain proteins. The molecular weight (kDa) of proteins is labeled on the left side of the membrane. (*B*–*G*) Original blots of Ferritin (*B*), TfR1 (*C*), TF (*D*), GPX4 (*E*), xCT (*F*), and GAPDH (*G*). The same samples were used for the above blots and the same GAPDH (*G*) was used for quantification.

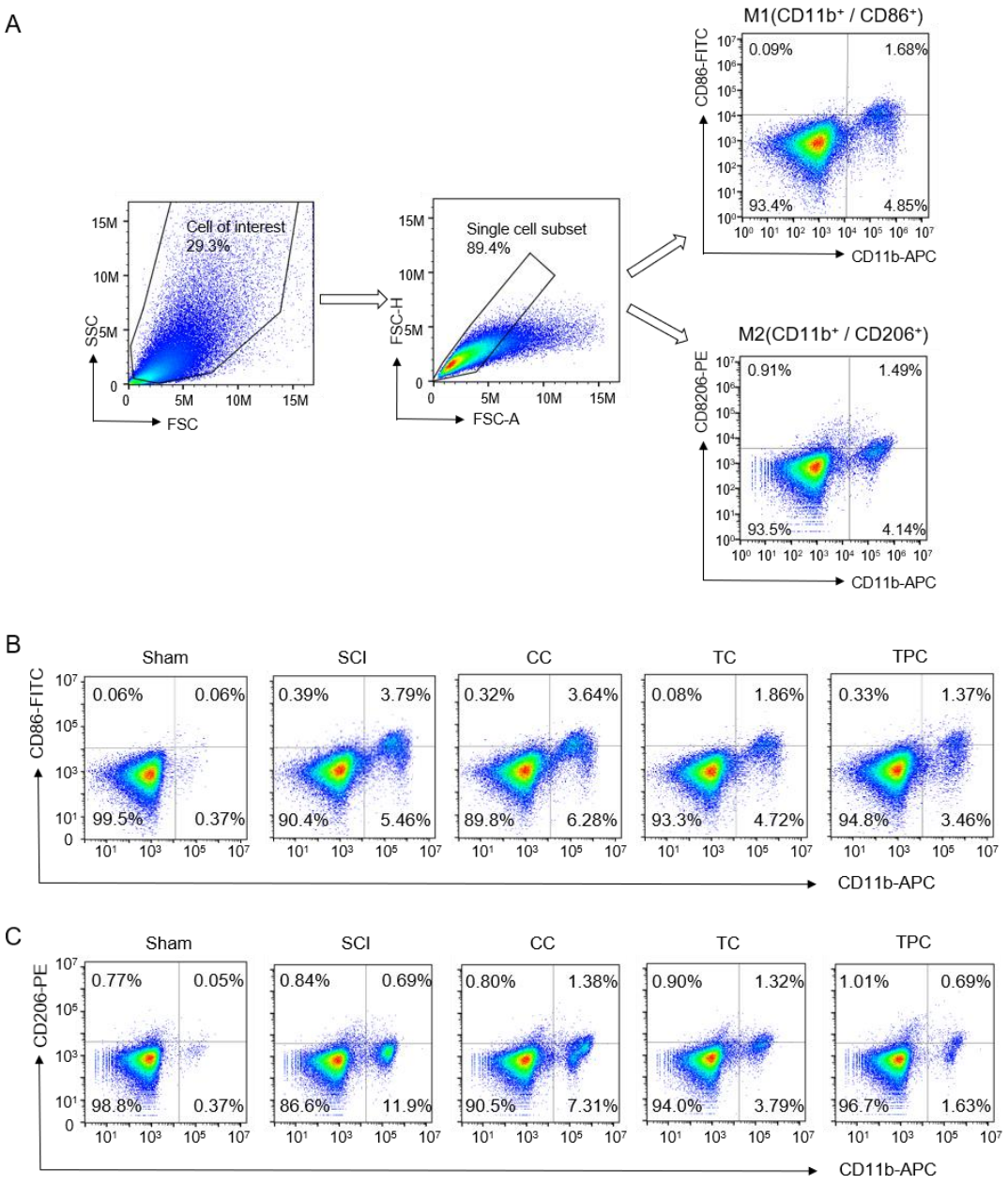

Fig. S30. (*A*) Sequential gating of Fig. 5 *F* and *G*. (*B* and *C*) Flow cytometric analysis of CD11b/CD86-positive cells (*B*) and CD11b/CD206-positive cells (*C*).

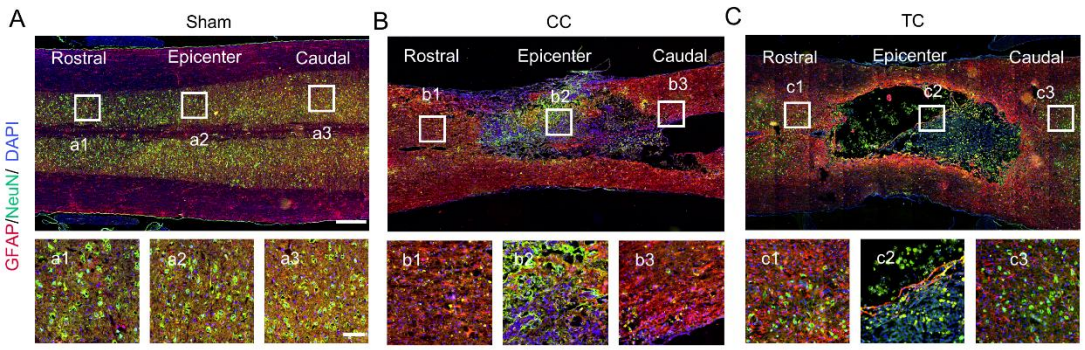

Fig. S31. (*A*–*C*) Representative immunostaining images of lesion sites of the (*A*) Sham, (*B*) CC, and (*C*) TC groups stained with anti-NeuN antibodies (red), anti-GFAP antibodies (green), and DAPI (blue). White boxes indicate the rostral border (a1, b1, and c1), epicenter (a2, b2, and c2), and caudal border (a3, b3, and c3) of injured spinal cords. Enlarged images of the box regions are shown in the bottom panel. Scale bar: 500 μm (top) and 100 μm (bottom).

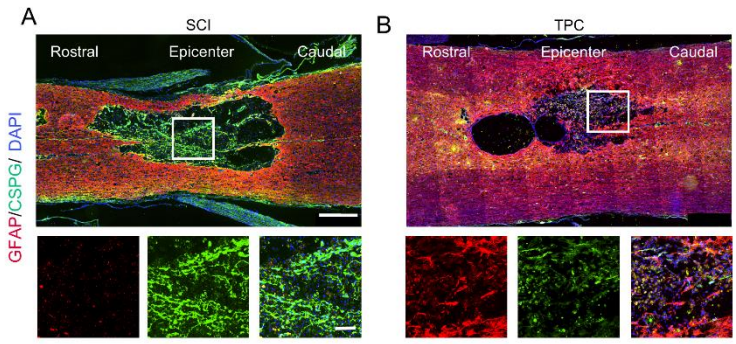

Fig. S32. (*A* and *B*) Representative immunostaining images of lesion sites of the (*A*) SCI and (*B*) TPC groups stained with anti-GFAP antibodies (red), anti-CSPG antibodies (green), and DAPI (blue). Scale bar: 500 μm (top) and 100 μm (bottom).

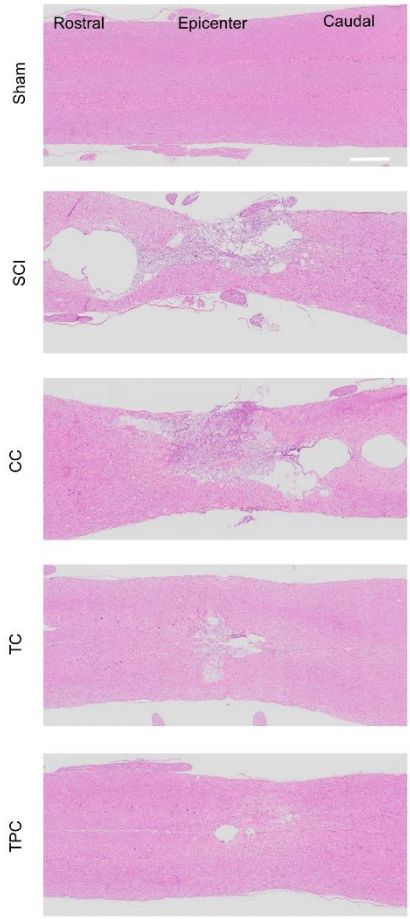

Fig. S33. Representative H&E images of longitudinal spinal cord sections in different groups. Scale bar: 500 μm.

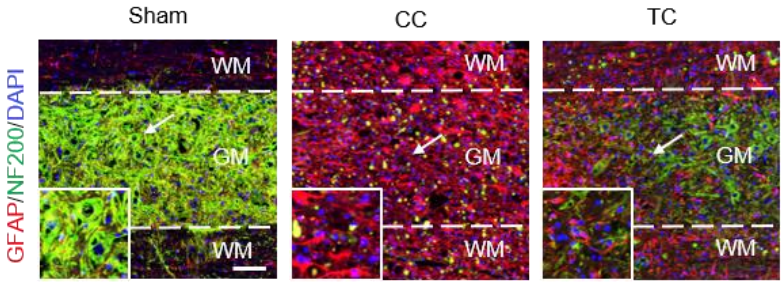

Fig. S34. Representative immunostaining images of lesion areas in the Sham, CC and TC groups at 8 wpi, stained with anti-NF200 (red)/anti-GFAP antibodies (green)/DAPI (blue). Scale bar: 50 μm. GM, gray matter. WM, white matter. An enlarged view of the box region is shown on the bottom left. The distance of the selected sites from the epicenter of injured spinal cords is 1.5 mm.

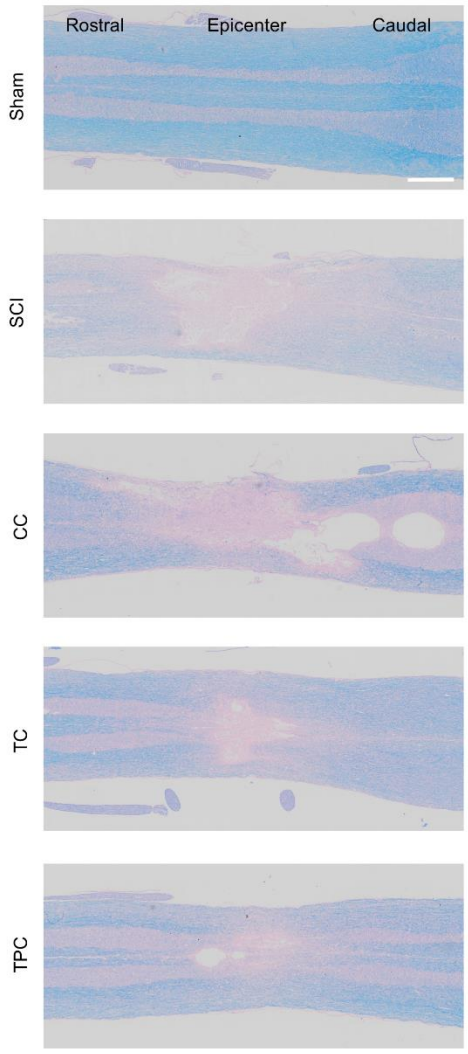

Fig. S35. Representative LFB images of longitudinal spinal cord sections in different groups. Scale bar: 500 μm.

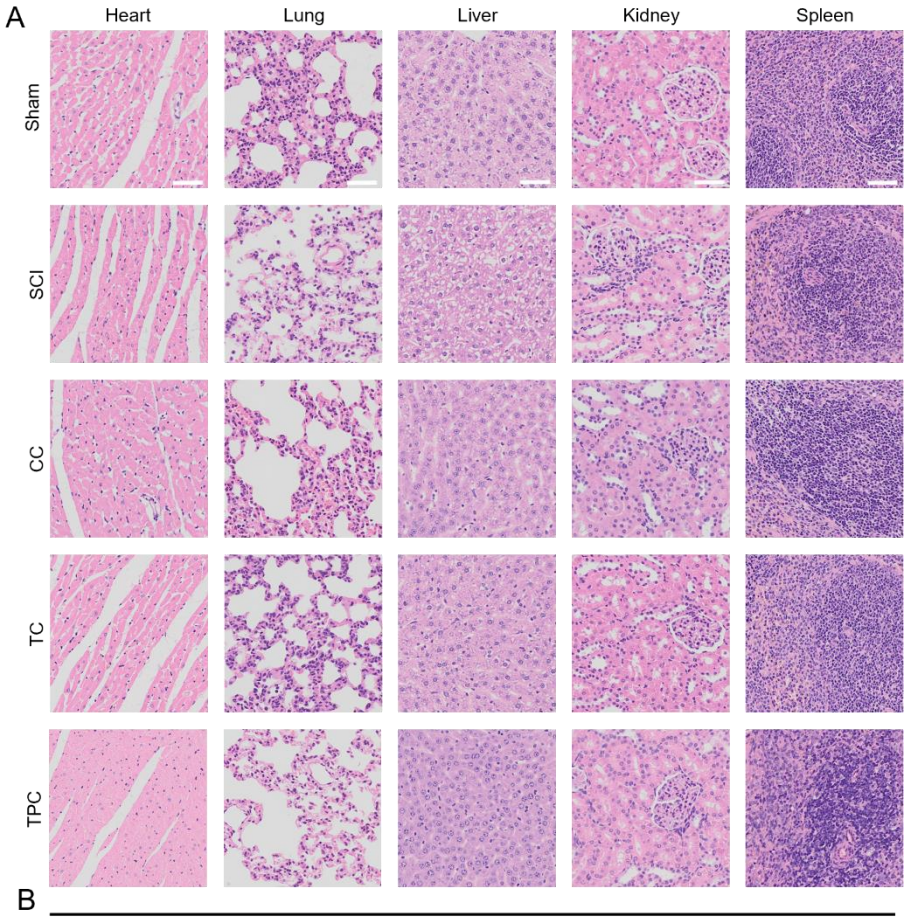

B

	Sham	SCI	CC	TC	TPC
ALT (U/L)	50.98 ± 15.52	103.16 ± 1.65	50.62 ± 16.72	49.43 ± 7.18	48.35 ± 0.50
AST (U/L)	139.96 ± 33.89	200.74 ± 4.33	188.68 ± 51.06	116.25 ± 9.40	110.25 ± 0.74
DBIL (μmol/L)	3.86 ± 0.98	17.88 ± 1.00	8.86 ± 0.38	7.41 ± 0.05	5.25 ± 0.22
TBIL (μmol/L)	7.40 ± 0.90	33.43 ± 1.37	18.28 ± 0.12	16.19 ± 0.23	11.6 ± 0.26
BUN (mg/dL)	21.41 ± 0.20	46.27 ± 0.72	28.94 ± 0.46	18.37 ± 0.24	29.15 ± 0.47
Crea (μmol/L)	42.27 ± 0.58	39.10 ± 1.42	40.11 ± 2.16	35.26 ± 0.96	29.97 ± 0.79
Urea (μmol/L)	75.42 ± 5.94	146.6 ± 10.96	103.5 ± 3.41	95.99 ± 6.98	52.58 ± 8.10

Fig. S36. (*A*) Representative H&E images of heart, lung, liver, kidney and spleen in different groups. Scale bar: 50 μm. (*B*) Blood test results of various groups (n = 3). All data represent the mean ± SD. ALT, alanine aminotransferase. AST, aspartate transaminase. DBIL, direct bilirubin. TBIL, total bilirubin. BUN, blood urea nitrogen. Crea, creatinine.

Table S1. RT-qPCR primers.

Rattus gene	Primer	Sequence (5'-3')
Tuj-1	Forward	CAACTATGTGGGGACTCGG
	Reverse	TGGCTCTGGGCACATACTTG
Gfap	Forward	TTGACCTGCGACCTTGAGTC
	Reverse	GAGTGCCTCCTGGTAACTCG
NeuroD1	Forward	AGCCCCCTAACTGATTGCAC
	Reverse	TCGGTGGATGGTTCGTGTTT
Chat	Forward	TCTGCTGTTATGGACCCGTG
	Reverse	GCAAACTCCACAGACGAGGT
Scn1a	Forward	TAACCTCAGCCAAACCAGCA
	Reverse	AGTTGTTCCATTGTCATCAGTAGC
Trpc5	Forward	TATCCTCACAGCATTCCGGC
	Reverse	TCTTCGCTGTGGTCATCTCG
Hapln4	Forward	GCTACCCCATCGTGAATCCG
	Reverse	GTAGACACCGAAGAGGCGAC
Hoxc10	Forward	ACCGAACATCTGGAATCGCC
	Reverse	CGTTCCTTTTCGCTCTCCGA
Efna3	Forward	GGCATGCGGTATACTGGAACA
	Reverse	AGTCGTTCACGTTCACTTGC
Gapdh	Forward	TCTCTGCTCCTCCCTGTTCT
	Reverse	ATCCGTTCACACCGACCTTC
Gpx4	Forward	CTCGCAATGAGGCAAAACCG
	Reverse	GGGAAGGCCAGGATTCGTAA
Dmt1	Forward	TGGCAGTGTTTGATTGCGTT
	Reverse	CCGCTGGTATCTTCGCTCA
Fsp1	Forward	GGGAGAAGGACAGACGAAGC
	Reverse	TCTTCCGGGGCTCCTTATCT
Ireb2	Forward	CTCCCCAAGTGCAGGATACA
	Reverse	GCAGCTTCCAATAGGACCCG
TfR1	Forward	TGAGGAACCAGACCGCTACA
	Reverse	CACACTGGACTTCGCAACAC

Section 3. Legends for Movies S1–S3

Movie S1. Representative locomotor performance of rats in Control, CC, TC and TPC groups at 1 wpi.

Movie S2. Representative locomotor performance of rats in Control, CC, TC and TPC groups at 4 wpi.

Movie S3. Representative locomotor performance of rats in Control, CC, TC and TPC groups at 8 wpi.

Section 4. SI References

1. P. Yang, Z. Gu, F. Zhu, Y. Li, Structural and functional tailoring of melanin-like polydopamine radical scavengers. *CCS Chem.* 2, 128–138 (2020).
2. T. Li, Z. Liu, J. Hu, L. Chen, T. Chen, Q. Tang, B. Yu, B. Zhao, C. Mao, M. Wan, A universal chemotactic targeted delivery strategy for inflammatory diseases. *Adv. Mater.*, e2206654 (2022).
3. J. Zhang, C. Chen, A. Li, W. Jing, P. Sun, X. Huang, Y. Liu, S. Zhang, W. Du, R. Zhang, Y. Liu, A. Gong, J. Wu, X. Jiang, Immunostimulant hydrogel for the inhibition of malignant glioma relapse post-resection. *Nat. Nanotechnol.* 16, 538–548 (2021).
4. H. Geng, Q. Z. Zhong, J. Li, Z. Lin, J. Cui, F. Caruso, J. Hao, Metal ion-directed functional metal–phenolic materials. *Chem. Rev.* 122, 11432–11473 (2022).
5. H. Ejima, J. J. Richardson, K. Liang, J. P. Best, M. P. van Koeverden, G. K. Such, J. Cui, F. Caruso, One-step assembly of coordination complexes for versatile film and particle engineering. *Science* 341, 154–157 (2013).
6. M. A. Rahim, K. Kempe, M. Müllner, H. Ejima, Y. Ju, M. P. van Koeverden, T. Suma, J. A. Braunger, M. G. Leeming, B. F. Abrahams, F. Caruso, Surface-confined amorphous films from metal-coordinated simple phenolic ligands. *Chem. Mater.* 27, 5825–5832 (2015).
7. E. Degtyar, M. J. Harrington, Y. Politi, P. Fratzl, The mechanical role of metal ions in biogenic protein-based materials. *Angew. Chem. Int. Ed.* 53, 12026–12044 (2014).